

Soluble Antigen Arrays utilize molecular and physical features to suppress Experimental
Autoimmune Encephalomyelitis

By

Copyright 2011

Joshua Orion Sestak

Submitted to the graduate degree program in Pharmaceutical Chemistry
and the Graduate Faculty of the University of Kansas in
partial fulfillment of the requirements for the degree of
Doctor of Philosophy.

Cory J. Berkland, Committee Chairperson

Teruna J. Siahaan

C. Russell Middaugh

Jeff Krise

Charlotte M. Vines

Date Defended: July 1, 2011

The Dissertation Committee for Joshua Orion Sestak
certifies that this is the approved version of the following dissertation:

Soluble Antigen Arrays utilize molecular and physical features to suppress Experimental
Autoimmune Encephalomyelitis

Cory J. Berkland, Committee Chairperson

Teruna J. Siahaan

C. Russell Middaugh

Jeff Krise

Charlotte M. Vines

Date approved: July 1, 2011

To God and my Family
Without your understanding, patience, and forgiveness I would never have arrived at this
destination

Acknowledgements

I would like to express my sincerest gratitude and appreciation to my advisor and mentor, Cory Berkland, for taking a chance on a “rogue” first year graduate student, and allowing me to explore my inner creativity. He gave me the freedom to discover, the resources to support, and the confidence to succeed. His faith and dedication to his graduate students, his work, and to his family, inspired me to put in the extra hours, days, and weeks to try and do something unique, and provided me with an example of the researcher I hope to become,.

To all my colleagues and collaborators at the University of Kansas I express my extreme gratefulness for their contributions to my project success, or simply my sanity: Jeff Aube, Patrick Porubsky, Justin Thomas, Talia Martin, Griffin Roberts, Cameron Siler, Ahmed Badawi, Barlas Buyuktimkin, Chris Kuehl, Sharadvi Thati, Nashwa El-Gendy, Chuda Chittasupho, Supang Khondee, Amir Fakhari, Abdul Baoum, Sheng-Xue Xie, Huili Guan, Mark Bailey, Kristin Aillon, Taryn Bagby, Sara Rosen, Scott Archer Mitchell, Kyle Mendenhall, and Rob Hicklin.

To my past mentors, teachers, and colleagues who encouraged, inspired, and helped facilitate my pursuit of a graduate science career I say thank you: Jeff Cronk, Nancy Staub, Rick Costantino, Alexis Kays Leonard, Lalit Peddakota, and Michael Ferguson. The opportunities, encouragement, and guidance have been invaluable. To my Gnomies: Matthew Hoag, Scott Friedrich, Mat Rockafeld, Jeff Hyatt, and Dave McMartin, I promise to never let you down.

I am sincerely grateful to Al and Lila Self, whose vision and extreme generosity helped form the Madison and Lila Self Graduate Fellowship and provided myself and many other students with an experience that cannot be matched by any graduate program. I came to KU because of Al Self’s vision and can only hope to achieve a level of success that would make Al and Lila proud. Additionally, I would like to thank current and former Self Graduate Fellowship staff for their dedication to the fellows and the development program: Howard Mossberg, Cathy Dwigans, Sharon Graham, Patty Dannenberg, and Jim Morrison.

I am also indebted to the Institute for Advancing Medical Innovation (IAMI) for the opportunities and growth that it has provided me during the two years I have been a fellow. During my fellowship they have exposed me to a whole new world beyond science. While many times it felt as if I were drinking from a fire hose, the experiences I had during my tenure within IAMI have made me a more educated and confident entrepreneur. Within IAMI I would like to thank staff, adjunct faculty, and fellows: Elizabeth Friis, Scott Weir, Paula Bullock, Marilyn Helms, Karl Strohmeier, Ken Lind, and Andrew Parkinson.

I would also like to thank the present and past members of my Master and Doctoral dissertation committees: Teruna Siahaan, Russ Middaugh, Jeff Krise, Michael Detamore, and Charlotte Vines. You have guided and challenged me throughout my graduate career and were instrumental in shaping my dissertation project.

Finally, I would like to thank God and my family for their undying and unwavering support, patience, and forgiveness. To my mother, Susan Sestak, thank you for being one of the most patient people I know, and always believing in me whether it made sense or not. To my father, Timothy Sestak, while a hard ass, continually challenging me to be better has made me the man I am today. To my brother, Zachary Sestak, thank you for providing me with inspiration and creativity. To my son Teigan, thank you for giving me a life balance that was much needed and for teaching me there is never a bad day to go to the park. To BlackJack, no matter what happened in life you were always happy and some days there is nothing better than a happy dog. Most importantly, thank you to Lacy for being my partner and teammate throughout this experience and into our future endeavors. Your encouragement, support, and willingness to put up with me when I was having a bad day gave me more strength than you can ever imagine.

Joshua Orion Sestak

July 1, 2011

Table of Contents

Chapter 1: Background and Introduction to Thesis

- 1.1 Nanomaterials and Immune Response
- 1.2 Peripheral Delivery and Inflammatory Response: Vaccines
- 1.3 Antigen Presentation and Immune Response: “Dintzis’ Rules”
- 1.4 Transport of Nanomaterials
- 1.5 Lymphatic Delivery and Tolerant Response: Immune Therapy
- 1.6 Synergizing recent *in vitro* studies with “Dintzis’ Rules”
- 2.1 Introduction of thesis
- 2.2 BPI vs. Polymer based SAgA
 - 2.2.1 Design of Thesis

Chapter 2: Synthesis and characterization of SAgAs

- 2.1 Introduction
- 2.2 Materials and Methods
- 2.3 Results and Discussion
- 2.4 Conclusions

Chapter 3: Evaluation of SAgA efficacy and effect of SAgA scaffold

- 3.1 Introduction
- 3.2 Materials and Methods
- 3.3 Results
- 3.4 Discussion
- 3.5 Conclusions

Chapter 4: Optimization of SAgAs – Effect of target and size

- 4.1 Introduction
- 4.2 Materials and Methods
- 4.3 Results
- 4.4 Discussion
- 4.5 Conclusions

Chapter 5: Conclusions and Future Directions

Abstract

Blockade of immune cell adhesion during antigen recognition may suppress the inflammatory immune response in autoimmune diseases. Employing a novel *N*-oxime chemistry, Soluble Antigen Arrays (SAGAs) were synthesized to simultaneously display intracellular cell-adhesion molecule-1 (ICAM-1) inhibitor and antigen. Hyaluronic acid (HA) was used as a backbone and two peptides were grafted, an ICAM-1 inhibitor (LABL) derived from α_L -integrin and an encephalitogenic epitope of proteolipid protein (PLP). Mice with experimental autoimmune encephalomyelitis (EAE) that received subcutaneous (s.c.) injections of SAGAs displaying both peptides showed significantly lower clinical disease scores and incidence, as well as better body weight maintenance than those treated with HA polymer alone. Multivalent presentation of cell-adhesion inhibitor (LABL) alone or antigen (PLP) alone was also evaluated. Treatment with hyaluronic acid grafted with only PLP antigen or only LABL peptide did not provide significant disease suppression and, in the case of LABL, actually exacerbated the disease. When hyaluronic acid was replaced with a PLGA nanoparticle displaying grafted LABL and PLP (NP-Array_{LABL-PLP}), an analogous treatment strategy with the NP-Array_{LABL-PLP} did not provide significant EAE suppression.

Next, the effect of SAGA molecular weight and cell-adhesion molecule target were evaluated. SAGAs with inhibitors targeting intracellular cell-adhesion molecule-1 (ICAM-1) or its ligand leukocyte-associated function antigen-1 (LFA-1) were equally effective. Also, the disease onset was delayed and severity was significantly reduced when the molecular weight of the SAGA was decreased. Animal imaging suggested that the smaller SAGA drained from the injection site more quickly than the larger SAGA, which may suggest enhanced transit to the regional lymphatics. Analysis of the cytokine production profiles of all treatments demonstrated that reducing SAGA size also provided the largest change in inflammatory cytokine response. SAGA performance, therefore, depended on lymphatic drainage as dictated by size, as well as molecular signaling resulting from co-grafting cell-adhesion inhibitor and antigen. Future

research should attempt to correlate SAgA transport with efficacy and explore the effect of grafting different inhibitors or activators of co-stimulation.

Chapter 1

Background and Introduction to Thesis

1.1 Nanomaterials and Immune Response

The use of nanomaterials such as polymers and colloids in medicine and biotechnology has grown dramatically over the past two decades. (1) While the applications vary greatly, many have explored the ability of these materials to generate an immune response. Nanomaterials have been used in vaccines to invoke a protective immune response, but less work has explored features for inducing tolerance. (2-3) The effect of particle size, drug loading, and toxicity of these materials is well documented for specific applications. (3) Outside of particle size however, the effect of nanomaterial physical characteristics and route of administration on transport, final deposition site, and immune response merits further exploration. In particular, research must probe the ability of nanomaterials presenting small molecules, peptides, or other haptens on or along their surface to illicit specific and sustained immune responses.

The importance of physical presentation of antigen is a well-documented effector of vaccine efficacy. Adjuvants are used to help generate immune responses against the delivered antigen and the way an adjuvant interacts with an antigen (e.g. surface adsorption, changes in protein folding, antigen epitope stability, and/or the physical formulation of the vaccine) is crucial to establishing potency and long term efficacy. (4-5) Even small changes to any of these factors can result in dramatic decreases in the clinical efficacy. (5) The physical and chemical context of antigen presentation is an important determinant of a vaccine's ability to generate an inflammatory response and achieve sustained immune protection.

Dintzis and others investigated the immune response to nanomaterials displaying multiple copies of grafted antigen, which demonstrated the importance of physical presentation on the magnitude and type of immune response. Dintzis developed "rules" for antigen-grafted polymers by manipulating grafting characteristics of small molecule or peptide haptens along flexible polymer chains, correlating structure to the immune response. (6-9) Using 'arrays' of antigen grafted to polymers ranging in size from 3 to 500 kDa, Dintzis systematically

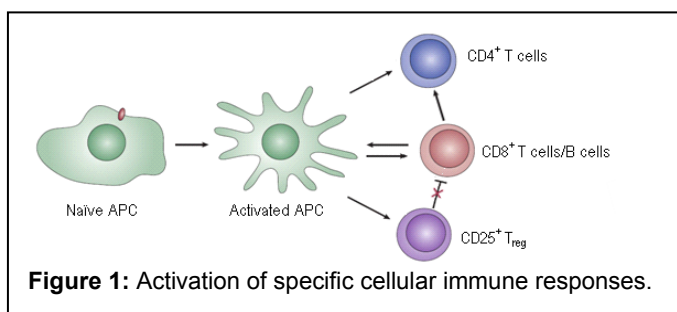
investigated the role that valency played on the material's ability to initiate specific immune responses. While the smaller arrays (~30 kDa) had a low binding avidity *in vitro*, they were typically more efficient in generating a tolerogenic immune response *in vivo*. (10) Dintzis hypothesized that array size played a role in differential signal transduction induced by the arrays on a cellular level. Building on these results, it was demonstrated that immune response could favor expansion of T cells or B cells by controlling factors such as total number and density of the haptens grafted along the polymer. (7, 9, 11)

More recent *in vitro* analysis of these "rules" has yielded slightly different results. In cell culture comprised of specific populations of target immune cells, larger therapeutic constructs with higher hapten density and stronger binding avidity often produced the largest cellular response. (12) This conflicting data resulting from *in vitro* studies suggested that additional elements must factor into the immune response generated *in vivo*. Deciphering these differences is complicated by the highly variable environment these polymeric nanomaterials experience when dosed by different routes. There is a need for transport of the nanomaterials away from or immune cells to the site of injection before immune activation can be achieved. Synergizing these findings suggests that nanomaterials indeed dictate the immune response via multivalent presentation of antigen, but also control the transport and localization *in vivo* to tailor immune response.

1.2 Peripheral Delivery and Inflammatory Response: Vaccines

Vaccines rely on the recruitment of immune cells to the site of injection to generate an effective immune response. (13-15) Professional antigen presenting cells (pAPCs) such as dendritic cells (DCs) must be recruited to the periphery, sample from the microenvironment, then migrate to the lymphatics where they may activate naïve lymphocytes. (16) The use of adjuvants or immunogenic vaccine particles can enhance recruitment, recognition, and uptake of the injected material by pAPCs. (4, 13) After uptake and processing of the vaccine antigen,

activation of the innate immune response further enhances recruitment of immune cells to the injection site (Figure 1). (13, 17-19)



Initial steps in immune activation include increased co stimulatory and antigen recognition capacities. Specifically, the surface density of cellular receptors such as cell-adhesion molecules and the major histocompatibility complex (MHC) is increased. The main functions of this up-regulation are to enhance recognition of pathogenic antigens and to prime $CD4^+$ and $CD8^+$ T cells to help initiate the adaptive immune response. After clonal expansion of T cell populations, interaction between T and B cells leads to B cell activation, expansion, and conversion to plasma cells responsible for antibody secretion. The circulating antibodies produced aid in the clearance of the detected pathogen. Direct interaction of activated DCs with $CD8^+$ T cells converts these T cells to cytotoxic lymphocytes (CTLs) and induces the secretion of signaling factors to down-regulate immunosuppressive $CD25^+$ regulatory T cells (T_{reg}). Adaptive immune cells differentiate into memory cells that prime the immune system in the event of a secondary exposure, thereby completing the immune response. (17-18, 20-21)

These steps encompass rudimentary fundamentals of the immune response. Multiple targets are available for therapeutics along these different arms. Research continues to explore adaptive priming as with vaccines and new trends in cancer therapy often aim to induce a selective pro inflammatory response (e.g. Th2). Induction of a tolerogenic immune response has also gained momentum; for example, T_{reg} production is desired in the case of autoimmunity where the body fails to differentiate self from non-self.

1.3 Antigen Presentation and Immune Response: “Dintzis’ Rules”

One of the key steps of immune activation is the presentation of antigen on the surface of pAPCs. After intracellular processing, the antigen is typically presented on the pAPC surface bound in the cleft of MHCs. Next, MHCs position themselves on the cellular surface with defined spacing and present the antigen with a specific orientation. (22) These spacing densities and antigen orientations help dictate the type of T cell (Th1 or Th2) or B cell response. While the antigen-MHC complex is difficult to recreate synthetically, nanomaterials can be constructed to emulate some of the antigen presentation characteristics.

Immune response can be maximized by recognizing distinct guidelines for recognition, processing, and clearance. Generally, materials with a Mw greater than 100 kDa and/or particle size of 50-5000 nm can be efficiently recognized and processed by dendritic cells and other pAPCs. (23-25) In addition to the initial recognition event, physical properties of the material will determine whether it is digested and/or cleared from the system and whether an immune response will be activated. (15) Similar to vaccines using adjuvants with adsorbed antigen, immune response to nanoparticles is dependent on the antigen type and display characteristics. (17-19) The number, density, and spacing of antigen plays an essential role in directing the immune response.

The importance of antigen display is perhaps best outlined in the work completed by Dintzis and others beginning in the late 1970's. (10, 26) “Haptens” (both small molecule and small peptide antigens) were systematically grafted (varying number and density) to polymers of discrete Mw. These antigen arrays were administered to animals IP, and the T cell or B cell responses were measured through cytokine or antibody production to characterize the immune response. (6-9, 11, 27-28) Hapten valance was critical to illicit an immune response, with materials displaying less than 10 haptens no longer generating a response. The immune response appeared to be driven by the hapten characteristics along the polymer backbone and

further investigation also suggested that there were critical spacing and density parameters to illicit specific cellular responses, independent of polymer Mw (Table 1).

Table 1: Material characteristics that produced the specified cellular response.

Effected Cells	Polymer Scaffold Mw (Da)	Total Estimated Haptens	Hapten per 1000 Da
T Cells	100,000	20	5
	30,000	7	4.3
	600,000 – 2,000,000	300 - 600	3.5 - 5
B Cells (Anti-TM Ab)	3,000	2	1.5
	14,000	7	2
	63,700	36	1.76

Much like the conserved sequences of pathogens that are recognized by pattern recognition receptors (PRRs), “Dintzis’ Rules” defined characteristics of soluble polymer constructs necessary for directing immune response:

- Valency of haptens: must be >10
- Spacing of haptens: 5-10 nm (50-100 Å)
- Rigidity of haptens: immobilization of receptor
- Binding kinetics and affinity

The results of work by Dintzis and others provided convincing evidence that nanomaterials can be synthesized to generate a specific immune response. We suspected that these findings also indirectly pointed to the role that transport plays in the immune response. Nanomaterial solubility, flexibility, and size all affect the ability of nanomaterials to either reside at or drain from the injection site. Additionally, location dictates the immune cell populations that the nanomaterials encounter.

1.4 Transport of Nanomaterials

The injection site plays a vital role in determining nanomaterial transport and final deposition site, which are important determinants of immune response. The three major parenteral administration routes are intravenous (IV), intramuscular (IM), and subcutaneous (SC). Each of these routes exposes the delivered nanomaterial to different initial and drainage environments. (29-30) While IV injection provides immediate systemic exposure; both IM and SC administration require the material to drain away from the injection site before entering into systemic or lymphatic circulation. Consequently, the nanomaterial properties and the local environment will determine the drainage kinetics from the injection site and the potential for retention at the injection site or accumulation in the lymph or blood pool.

Intravenous administration provides the optimal delivery route to give a dose quickly into systemic circulation. Distribution is rapid, however, IV injection immediately exposes materials to circulating lymphocytes, digestive enzymes, and proteins found in the blood as well as first pass metabolism, which can lead to rapid clearance. Materials below ~65 kDa or ~10 nm will show rapid renal clearance while larger materials may proceed to the spleen. (31) The spleen serves as an immunologic filter for the blood. Comprised of dendritic cells, natural killer cells, macrophages, B cells, T cells and red blood cells, the spleen captures foreign materials (e.g. antigens) from the blood. Additionally, circulating lymphocytes capture foreign materials and bring them to the spleen for presentation to T and B cells. Exposure to enzymes, renal and splenic clearance, antibody clearance, and other clearance mechanisms may make IV an undesirable choice for delivery of therapeutics that modulate immune response.

Delivery of nanomaterials via IM injection is preferred over SC in cases where large volumes of a drug product are required. The vaccine or therapeutic is usually injected into the upper arm, thigh, or buttock where the muscle is dense. The major factor in drug absorption after IM injection is the relative blood supply to the muscle where decreased blood supply extends the absorption time. Additionally, systemic exposure is often achieved only after the

materials pass through the draining lymph nodes. (32) In particular, the lymph readily takes up high molecular weight complexes, particles, and macromolecules, while smaller materials (e.g. < 10 nm) are more likely to be transported directly to the blood. (33-34) Drug can reside at the injection site for prolonged periods of time if the drug is large or partially immobilized (e.g. adsorbed on an adjuvant). As a result, the extended residence time may favor a peripheral immune response mediated by DC and macrophage migration to the site of injection.

Subcutaneous delivery is achieved through injection of the nanomaterials into fatty tissue just beneath the skin. The subcutaneous space allows drainage away from the injection site depending on the relative size of the therapeutic or “carrier.” Nanomaterials most likely will have one of three fates: 1) smaller materials (<10 nm) tend to drain to capillaries and into systemic circulation, 2) larger materials favor drainage into local lymphatic circulation and to secondary lymphoid organs, or 3) materials > 70 nm typically will remain at the injection site. (35-37) Therefore, immune modulating nanomaterials can be manufactured to take advantage of the subcutaneous drainage profile to provide optimal exposure to lymphatics and to minimize systemic exposure or peripheral immune response.

1.5 Lymphatic Delivery and Tolerant Response: Immune Therapy

The lymph nodes provide various immunological environments with specific cellular populations sequestered in different compartments. Within secondary lymphoid organs (e.g. lymph nodes and spleen), a very highly structured architecture exists that provides efficient induction of an immune response. (38-39) This microenvironment in lymph nodes can be characterized into three distinct subunits: (1) an antigen sampling compartment rich in pAPCs that process and present antigens to (2) T cells within the paracortex or (3) B cells in the lymph node cortex containing B cell follicles. This high level of organization helps to enhance cell-cell signaling and increases the probability of pAPCs encountering immune cells and antigen by bringing these populations together in a small volume environment. (38) Immune response is

driven in part by cell interactions within the lymph nodes which can induce responses through clonal expansion of cytokine-producing and cytotoxic T cells as well as through production of high-affinity antibodies. (40) The high concentration of immune cells as well as the efficient induction of immune response makes intra-lymphatic immunization very attractive for cancer vaccines. (41-44) In addition, direct injection of allergens into the lymph nodes has successfully induced tolerance toward specific allergens. (39) Traditional methods to promote tolerance toward specific allergens required multiple SC injections of the same allergen at low concentration over the course of years. Recent clinical trials have demonstrated that delivery of the allergen directly into the lymph nodes resulted in rapid tolerization toward the allergen. (39-40, 45-46)

While the therapeutic applications appear to vary greatly, each tolerization strategy looks to take advantage of initiating an immune response by delivering extremely small amounts of “antigenic” material. Promising results in the clinic suggest that delivery of materials into the lymph nodes whether through direct injection or drainage provides rapid exposure to a high concentration of immune cells. This can elicit a quick and/or large immune response toward the delivered materials. In many cases, the immune response can be directed toward antigen tolerance and not stimulation, a characteristic that is highly desirable in treating autoimmune diseases.

1.6 Synergizing recent *in vitro* studies with “Dintzis’ Rules”

The work of Dintzis provides strong and convincing evidence that antigen arrays can provide selective immune stimulation, however, as these “rules” were analyzed *in vitro* there appeared to be a deviation from *in vivo* results. The work of Kiessling and others aimed to correlate *in vivo* activities of multivalent antigens seen by Dintzis, with affects on B cell receptor (BCR) localization and signal transduction in B cells. (47) The studies focused on the ability of antigen arrays of large (500 haptens) and small (10 haptens) valencies to cluster surface

receptors and initiate an antibody response. The *in vitro* data did not support the claims made by Dintzis and Kiessling argued that it was the ability to cluster BCRs that was critical in signal amplification and antibody production. When tested, both the 500 hapten and 10 hapten arrays led to a high degree of BCR clustering (Figure 2), however, the resultant antibody production differed between the two populations.

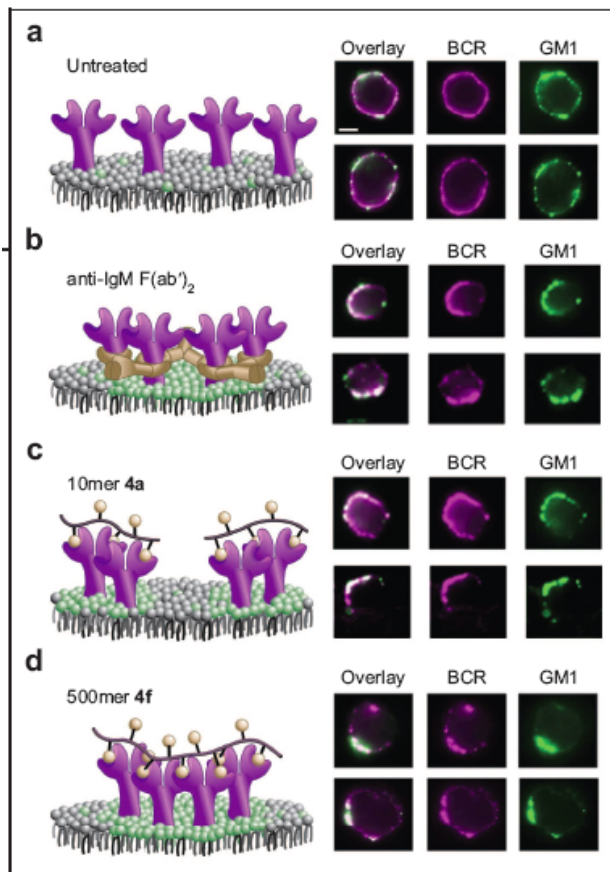


Figure 2: Visualization of BCR and glycosphingolipids localization on cell surfaces treated with multivalent ligands. BCR (purple) and glycosphingolipids (green) were overlaid and showed a high level of co-localization for both 10- and 500-hapten arrays. (47) Reproduced with permission.

In a different study, Chittasupho and others used primary DCs primed with ovalbumin antigen to analyze the ability of nanoparticles displaying multiple copies of inhibitors of intracellular adhesion molecule-1 (ICAM-1) or lymphocyte function-associated antigen (LFA-1) to block binding of T cells to DCs. The presentation of cell-adhesion ligands as multivalent arrays on the nanoparticle surface was hypothesized to enhance binding avidity and trigger

endocytosis of receptors, thereby blocking DC receptors and altering response better than free inhibitors. Molecular staining of ICAM-1 and LFA-1 demonstrated each receptor was expressed on the surface of DCs. Pretreatment of DCs with nanoparticle arrays (targeting either ICAM-1 or LFA-1) showed a >75% decrease in T cell conjugate formation with DCs compared to no treatment. Similar to the work of Kiessling, the effect of receptor binding and clustering on cell proliferation and cytokine response was measured. Although binding of DCs and T cells was inhibited to a similar extent by NPs displaying LABL or IBR, the resulting effect of the binding events was vastly different. Compared to controls, T cell proliferation was arrested when T cells were incubated in the presence of DCs treated with LABL-NPs (targeting ICAM-1), whereas DCs treated with IBR-NPs (targeting LFA-1) dramatically stimulated T cell proliferation. Similarly, the cytokine profiles differed greatly for LABL-NPs compared to IBR-NPs with regards to the amount of IL-6 or IL-17 varying depending on NP type.

These *in vitro* studies showed differing results in regards to cell surface receptor clustering and immune response for B cells (Kiessling and others) and T cells (Chittasupho and others). In Kiessling's model, BCR clustering was similar with treatment using different Mws of antigen arrays; however, each treatment produced different antibody production. Similarly, Chittasupho and others observed NPs displaying different cell-adhesion inhibitors produced equal amounts of binding and cellular uptake with drastically different cell proliferation and cytokine responses. These studies provide a look into how multivalent materials are interacting on the molecular and cellular level for specific immune cell subpopulations, but they are conducted on homogenous populations of immune cells *ex vivo*. A potential explanation for the observed disagreement with Dintzis' *in vivo* observations is that *in vitro* analysis provides the opportunity for all the tested materials to interact with the target cells. When delivered *in vivo*, the larger materials will most likely remain at the site of injection and not drain to the nodes where naïve T and B cells reside. Even so, the individual subpopulation differences provide

insight into what may be achieved if these nanomaterials are efficiently delivered to specific B or T cell populations *in vivo*.

2.1 Introduction of thesis

A specific cellular immune response can be achieved by particle or polymer nanomaterials displaying multiple copies of an antigen. The factors directly responsible for the response are still a matter of contention. *In vitro* studies provide an argument that the clustering event of cellular receptors and formation of an immunological synapse are essential in activating a potent cellular response. Studies with allergen tolerization therapies, however, have shown that it is not only necessary for the body to recognize the immunogenic material, but also where the material is recognized is key to rapid tolerance induction. Nanomaterials provide a unique scaffold that can be synthesized to address both molecular presentation motifs as well as Mw cutoffs to promote localization of the materials in lymph nodes. The arrays investigated by Dintzis, Kiessling, and Chittasupho displayed a single hapten along the manufactured nanomaterial. Research into enhancing the potency of T cell activation demonstrates that multiple signals and the number (valency), pattern, and translocation of these signals are direct contributors to the strength and type of immune response. (48-49) Nanomaterials that present antigen accompanied by a co stimulatory signal or cell-adhesion inhibitor provide yet another treatment strategy for traditional vaccines or tolerization therapy.

2.2 BPI vs. Polymer based SAgA

Previous research demonstrated that fusion of a cell-adhesion antagonist and disease-specific antigen in the form of a “bi-functional peptide inhibitor” (BPI) suppressed autoimmune disease in multiple models, including experimental autoimmune encephalomyelitis (EAE). (50-53) Efficacy of the BPI is proposed to be achieved through the ability of the inhibitor to disrupt the formation of the immunological synapse and, therefore, prohibit the activation or clonal

expansion of specific immune cell populations. Its small size (~3000 kDa) would theoretically result in a large systemic concentration after SC injection due to rapid absorption into the blood, unless the BPI binds to receptors at or near the injection site. Systemic exposure may result in accumulation in the spleen where the immune cell population would vary greatly when compared to lymphatics that drain the disease site.

Our research looked to build upon the success of BPI by expanding this construct to a polymer chain to create a “soluble antigen array” (SAgA). The SAgAs were designed to take advantage of “Dintzis Rules” for hapten spacing and density to maximize the immune response against the disease antigen. SAgAs were synthesized to simultaneously display peptides that inhibit the binding of ICAM-1 (LABL), or LFA-1 (IBR) alongside the EAE peptide antigen derived from proteolipid protein (PLP). Both hyaluronic acid (HA) and PLGA nanoparticles were evaluated as scaffolds to display the peptides, which were covalently grafted to HA via a novel *N*-oxime chemistry. In addition to antigen and cell-adhesion display, SAgA size was designed to promote local lymphatic drainage after SC injection, thus minimizing systemic exposure or retention at the injection site. (34-36)

Targeting the lymphatics provides SAgAs the optimum ability to influence immune response. SAgAs were, therefore, designed to promote rapid uptake into the local lymphatic structures and to extend the residence time within these structures. Previous results by Forrest and others, demonstrated that hyaluronic acid showed lymphatic uptake and increased the efficacy of the grafted therapeutics, while decreasing systemic exposure and toxicity. (54-55) Unpublished results from the Forrest lab by Meyer and others, also demonstrated that a linear relationship between size and drainage kinetics did not exist, rather there was an optimum Mw (~75 kDa) of HA to achieve rapid drainage into lymphatic circulation and avoid systemic exposure after SC injection. An outline of the design characteristics for SAgAs and rationale is shown in Table 2.

Table 2: Target characteristics and rationale for the design of SAgAs.

Structural Element	Rationale
Molecular Signaling	Presentation of antigen and cell-adhesion inhibitor simultaneously, increases the suppression ability of the therapeutic
Antigen Array	Optimize the hapten number and density along nanomaterial to increase ability to interact with cell surface receptors
Size	Control drainage characteristics to promote lymphatic drainage and increase interaction with target immune cells

2.2.1 Design of Thesis

The work outlined in this thesis encompasses the synthesis, physical characterization, and *in vivo* testing of SAgAs developed to treat EAE, the murine model of multiple sclerosis (MS). These arrays were synthesized using a soluble hyaluronic acid polymer backbone or PLGA-NP scaffolds. An antigen peptide (PLP) and/or cell-adhesion inhibitor (LABL or IBR) were conjugated to each of these scaffolds. The resulting conjugates were characterized and then tested *in vivo* in the EAE mouse model to establish efficacy. Later studies focused on the effect of cell-adhesion target (ICAM-1 or LFA-1) and therapeutic size on the ability of the materials to suppress EAE, alter the drainage away from the point of injection, and induce specific cytokine responses.

Chapter 2: Synthesis and characterization of SAgAs

Peptides were conjugated to the HA scaffolds via novel *N*-oxime chemistry. This conjugation scheme eliminates the need for modification of reactants, harsh reaction conditions, and/or multi-step reactions. The *N*-oxime reaction pathway was validated through extensive studies of reaction product using mass spectroscopy, nuclear magnetic resonance spectroscopy, and Fourier transform infrared spectroscopy. After the chemistry was validated, SAgAs were synthesized and the relative Mw, peptide concentration, and reaction efficiency were calculated using analytical techniques such as Gel Permeation Chromatography and High Pressure Liquid Chromatography.

Chapter 3: Evaluation of SAgA efficacy and effect of SAgA scaffold

SAgAs were synthesized to display a cell-adhesion inhibitor (LABL) and antigen (PLP) peptides by conjugating the peptides to hyaluronic acid or PLGA-NPs. After characterization, the materials were injected SC into mice with EAE. All manufactured arrays were compared against a negative PBS and positive PLP-BPI control. Therapeutic efficacy was evaluated by measuring clinical score and body weight over 25 days. Further studies evaluated the effect of increasing dose and inhibitor type for comparison to controls including, LABL (cell-adhesion inhibitor) only, PLP (antigen) only, free LABL + PLP peptides, or free scaffold (HA vs. PLGA-NP).

Chapter 4: Optimization of SAgAs – Effect of target and size

To further optimize EAE suppression, SAgAs displaying an alternate cell-adhesion inhibitor (IBR) were synthesized. Additionally, SAgAs with lower Mw were synthesized to enhance drainage of the materials to the lymphatics. Clinical scores and body weight in the EAE mouse model were evaluated, and *in vivo* imaging of SAgAs and cytokine analyses were conducted. *In vivo* imaging was used to qualitatively track retention or drainage of SAgAs from the injection site. The circulating concentration of pro inflammatory (IFN- γ , TNF- α , and IL-2) and anti-inflammatory or tolerogenic (IL-4, IL-10, and IL-17) cytokines provided insight into the underlying immunological mechanisms of the immune responses.

References:

1. L Zhang FG, JM Chan, AZ Wang, RS Langer and OC Farokhzad. Nanoparticles in Medicine: Therapeutic Applications and Developments. *Clinical Pharmacology & Therapeutics*. 2008;83(5):761-9.
2. Brannon-Peppas L, Blanchette JO. Nanoparticle and targeted systems for cancer therapy. *Advanced Drug Delivery Reviews*. 2004;56(11):1649-59.
3. Klippstein R, Pozo D. Nanotechnology-based manipulation of dendritic cells for enhanced immunotherapy strategies. *Nanomedicine : nanotechnology, biology, and medicine*. 2010;6(4):523-9.
4. Cox JC, Coulter AR. Adjuvants--a classification and review of their modes of action. *Vaccine*. 1997;15(3):248-56.
5. Reed SG, Bertholet S, Coler RN, Friede M. New horizons in adjuvants for vaccine development. *Trends in immunology*. 2009;30(1):23-32.
6. Dintzis RZ MM, Dintzis HM. Inhibition of anti-DNP antibody formation by high doses of DNP-polyacrylamide molecules; effects of hapten density and hapten valence. *J Immunol*. 1985;135(1):423-7.
7. Siliciano RF CR, Keegan AD, Dintzis RZ, Dintzis HM, Shin HS. Antigen valence determines the binding of nominal antigen to cytolytic T cell clones. *J Exp Med*. 1985;162(2):768-73.
8. Symer DE DR, Diamond DJ, Dintzis HM. Inhibition or activation of human T cell receptor transfectants is controlled by defined, soluble antigen arrays. *J Exp Med*. 1992;176(5):1421-30.
9. Symer DE RJ, Dintzis RZ, Voss EW Jr, Dintzis HM. Durable elimination of high affinity, T cell-dependent antibodies by low molecular weight antigen arrays in vivo. *J Immunol*. 1995;155(12):5608-16.
10. Dintzis HM DR, Vogelstein B. Molecular determinants of immunogenicity: the immunon model of immune response. *Proc Natl Acad Sci U S A*. 1976;73(10):3671-5.
11. Reim JW SD, Watson DC, Dintzis RZ, Dintzis HM. Low molecular weight antigen arrays delete high affinity memory B cells without affecting specific T-cell help. *Mol Immunol*. 1996;33(17-18):1377-88.
12. Kiessling LL. Decoding Signals with Chemical Biology. *ACS Chemical Biology*. 2010;5(1):1-2.
13. Achal Pashine NMVJBU. Targeting the innate immune response with improved vaccine adjuvants. *Nature Medicine*. 2005;11:S63-S8.
14. RZ D. Rational design of conjugate vaccines. *Pediatr Res*. 1992;32(4):376-85.
15. Xiang SD, Scholzen A, Minigo G, David C, Apostolopoulos V, Mottram PL, et al. Pathogen recognition and development of particulate vaccines: Does size matter? *Methods*. 2006;40(1):1-9.
16. Villablanca EJ RV, Mora JR. Dendritic cell migration and lymphocyte homing imprinting. *Histology and Histopathology*. 2008;23(7):897-910.
17. Hoebe K, Janssen E, Beutler B. The interface between innate and adaptive immunity. *Nat Immunol*. 2004;5(10):971-4.
18. Medzhitov R, Janeway Jr CA. Innate immune recognition and control of adaptive immune responses. *Seminars in Immunology*. 1998;10(5):351-3.
19. Ulevitch RJ. Therapeutics targeting the innate immune system. *Nat Rev Immunol*. 2004;4(7):512-20.
20. Chinen J, Shearer WT. Basic and clinical immunology. *Journal of Allergy and Clinical Immunology*. 2005;116(2):411-8.
21. Nathalie Cools PP, Viggo F. I. Van Tendeloo, and Zwi N. Berneman. Regulatory T Cells and Human Disease. *Clinical and Developmental Immunology*. 2007;2007.

22. Murray JS. How the MHC selects Th1/Th2 immunity. *Immunology Today*. 1998;19(4):157-62.
23. Jang J LD, Choi IH. The impact of nanomaterials in immune system. *Immune Netw*. 2010;3:85-91.
24. Foged C, Brodin B, Frokjaer S, Sundblad A. Particle size and surface charge affect particle uptake by human dendritic cells in an in vitro model. *International Journal of Pharmaceutics*. 2005;298(2):315-22.
25. Thiele L, Merkle HP, Walter E. Phagocytosis and Phagosomal Fate of Surface-Modified Microparticles in Dendritic Cells and Macrophages. *Pharmaceutical Research*. 2003;20(2):221-8.
26. Dintzis HM DR. Antigens as immunoregulators. *Immunological Reviews*. 1990;115:243-50.
27. Hafler DA, Weiner HL. Immunologic Mechanisms and Therapy in Multiple Sclerosis. *Immunological Reviews*. 1995;144(1):75-107.
28. Watson DC RJ, Dintzis HM. Suppression of the antibody response to a polymorphic peptide from the platelet alloantigen integrin beta3 with low molecular weight antigen arrays. *J Immunol*. 1996;156(7):2443-50.
29. Greenblatt DJ, Shader RI, Franke K, Maclaughlin DS, Harmatz JS, Allen MD, et al. Pharmacokinetics and bioavailability of intravenous, intramuscular, and oral lorazepam in humans. *Journal of Pharmaceutical Sciences*. 1979;68(1):57-63.
30. Anya M. Hillery AWL, James Swarbrick, editor. *Drug Delivery and Targeting: For Pharmacists and Pharmaceutical Scientists*. London: Taylor and Francis; 2001.
31. Leon Shargel SW-P, Andrew B.C. Yu. *Applied Biopharmaceutics and Pharmacokinetics*. 5 ed: McGraw-Hill/Appleton & Lange; 2005.
32. Swartz MA, Hubbell JA, Reddy ST. Lymphatic drainage function and its immunological implications: From dendritic cell homing to vaccine design. *Seminars in Immunology*. 2008;20(2):147-56.
33. Kim CK, Han JH. Lymphatic delivery and pharmacokinetics of methotrexate after intramuscular injection of differently charged liposome-entrapped methotrexate to rats. *Journal of Microencapsulation*. 1995;12(4):437-46.
34. Takakura Y, Matsumoto S, Hashida M, Sezaki H. Enhanced Lymphatic Delivery of Mitomycin C Conjugated with Dextran. *Cancer Research*. 1984;44(6):2505-10.
35. Supersaxo A, Hein WR, Steffen H. Effect of Molecular Weight on the Lymphatic Absorption of Water-Soluble Compounds Following Subcutaneous Administration. *Pharmaceutical Research*. 1990;7(2):167-9.
36. Jagannath Kota KKM, Danielle N. McLennan, Glenn A. Edwards,, Christopher J. H. Porter aSAC. Lymphatic Absorption of Subcutaneously Administered Proteins: Influence of Different Injection Sites on the Absorption of Darbepoetin Alfa Using a Sheep Model. *Drug Metabolism and Disposition*. 2007;35(12).
37. Oussoren C, Zuidema J, Crommelin DJA, Storm G. Lymphatic uptake and biodistribution of liposomes after subcutaneous injection.: II. Influence of liposomal size, lipid composition and lipid dose. *Biochimica et Biophysica Acta (BBA) - Biomembranes*. 1997;1328(2):261-72.
38. Junt T, Scandella E, Ludewig B. Form follows function: lymphoid tissue microarchitecture in antimicrobial immune defence. *Nat Rev Immunol*. 2008;8(10):764-75.
39. Seraina von Moos TMK, Gabriela Senti. Novel Administration Routes for Allergen-Specific Immunotherapy: A Review of Intralymphatic and Epicutaneous Allergen-Specific Immunotherapy. *Immunology and Allergy Clinics of North America*. 2011;31(2).
40. Senti G, Johansen P, Kündig TM. Intralymphatic immunotherapy. *Current Opinion in Allergy and Clinical Immunology*. 2009;9(6):537-43 10.1097/ACI.0b013e3283310ff7.

41. Weber J, Boswell W, Smith J, Hersh E, Snively J, Diaz M, et al. Phase 1 Trial of Intranodal Injection of a Melan-A/MART-1 DNA Plasmid Vaccine in Patients With Stage IV Melanoma. *Journal of Immunotherapy*. 2008;31(2):215-23 10.1097/CJI.0b013e3181611420.
42. Ochsenbein AF. Immune surveillance against a peripheral solid tumour fails because of immunological ignorance. *Proc Natl Acad Sci USA*. 1999;96:2233-8.
43. Ochsenbein AF, Sierro S, Odermatt B, Pericin M, Karrer U, Hermans J, et al. Roles of tumour localization, second signals and cross priming in cytotoxic T-cell induction. *Nature*. 2001;411(6841):1058-64.
44. Kreiter S, Selmi A, Diken M, Koslowski M, Britten CM, Huber C, et al. Intranodal Vaccination with Naked Antigen-Encoding RNA Elicits Potent Prophylactic and Therapeutic Antitumoral Immunity. *Cancer Research*. 2010;70(22):9031-40.
45. Akdis CA, Akdis M. Mechanisms of allergen-specific immunotherapy. *Journal of Allergy and Clinical Immunology*. 2011;127(1):18-27.
46. Bousquet J, Lockey R, Malling H-J. Allergen immunotherapy: Therapeutic vaccines for allergic diseases A WHO position paper. *The Journal of allergy and clinical immunology*. 1998;102(4):558-62.
47. Puffer EB, Pontrello JK, Hollenbeck JJ, Kink JA, Kiessling LL. Activating B Cell Signaling with Defined Multivalent Ligands. *ACS Chemical Biology*. 2007;2(4):252-62.
48. Mossman KD, Campi G, Groves JT, Dustin ML. Altered TCR signaling from geometrically repatterned immunological synapses. *Science*. 2005;310(5751):1191-3.
49. Hartman NC, Nye JA, Groves JT. Cluster size regulates protein sorting in the immunological synapse. *Proc Natl Acad Sci U S A*. 2009;106(31):12729-34.
50. Satyanarayanajois SD, Büyüktimkin B, Gokhale A, Ronald S, Siahaan TJ, Latendresse JR. A Peptide from the Beta-strand Region of CD2 Protein that Inhibits Cell Adhesion and Suppresses Arthritis in a Mouse Model. *Chemical Biology & Drug Design*. 2010;76(3):234-44.
51. Manikwar P, Kiptoo P, Badawi AH, Büyüktimkin B, Siahaan TJ. Antigen-specific blocking of CD4-specific immunological synapse formation using BPI and current therapies for autoimmune diseases. *Medicinal Research Reviews*. 2011:n/a-n/a.
52. Naoki Kobayashi PK, Hitomi Kobayashi, Rahmawati Ridwan, Stefan Brocke, and Teruna J. Siahaan. Prophylactic and Therapeutic Suppression of Experimental Autoimmune Encephalomyelitis by a Novel Bifunctional Peptide Inhibitor. *Clinical Immunology*. 2008;129(1):69-79.
53. Murray JS, Oney S, Page JE, Kratochvil-Stava A, Hu Y, Makagiansar IT, et al. Suppression of Type 1 Diabetes in NOD Mice by Bifunctional Peptide Inhibitor: Modulation of the Immunological Synapse Formation. *Chemical Biology & Drug Design*. 2007;70(3):227-36.
54. Cai S, Xie Y, Davies NM, Cohen MS, Forrest ML. Pharmacokinetics and disposition of a localized lymphatic polymeric hyaluronan conjugate of cisplatin in rodents. *Journal of Pharmaceutical Sciences*. 2010;99(6):2664-71.
55. Cohen MS, Cai S, Xie Y, Forrest ML. A novel intralymphatic nanocarrier delivery system for cisplatin therapy in breast cancer with improved tumor efficacy and lower systemic toxicity in vivo. *The American Journal of Surgery*. 2009;198(6):781-6.

Chapter 2

Synthesis and characterization of SAgAs

2.1 Introduction

Oxime chemistry has emerged as a promising conjugation scheme that utilizes the highly specific reaction of aminoxy groups to aldehydes or ketones. (1-4) The reaction can be carried out in water and avoids harsh catalysts or reaction conditions. (5) In addition, aminoxy reactivity is significantly higher than primary amines, thus conferring the desired specificity for conjugation using polypeptides. (3, 6-7) One drawback to this approach has been the need for an aldehyde or ketone group to provide a reactive site. A characteristic that usually necessitates engineering the reactant.

Currently, synthetic glycoconjugation would benefit from simplified reaction schemes. (6) Polysaccharides and peptides cannot be exposed to many of the conditions required for traditional conjugation schemes (e.g. solvent, pH, temperature) due to stability concerns. (8) In addition, current approaches often utilize multiple steps, such as activation procedures to form reactive intermediates or the addition of linker molecules to facilitate stability or to improve reaction efficiency. (9) These encumbrances coupled with low product yields and lengthy purification procedures make many of the current glycoconjugation methods inconvenient for translational medicine or assays and impractical for scale-up. (9-10)

An additional roadblock in the synthesis of glycoconjugates is the inefficiency or variability of reactions. Research efforts may halt at the bench due to low reactivity, the need for catalysts, complex addition of reactive sites, and/or the use of undesirable solvents. Further problems emerge when conjugating multiple peptide species since small differences in reactivity may yield unpredictable molar ratios. (11) Such issues inhibit the exploration of multivalent or multifunctional polymers or colloids with defined ligand densities and ratios.

Oxime chemistry has historically focused on aldehyde or ketone reactions to aminoxy groups. (9) Here, aminoxy reactivity to the carbonyl carbon on *N*-acetyl amides was investigated as a unique approach to synthetic glycoconjugation. Specifically, *N*-acetyl glucosamine (NAG) was explored as a link to glycosylation or functionalization of glycosaminoglycans such as hyaluronic acid. (12-13)

2.2 Materials

N-acetyl glucosamine, glucuronic acid, *N*-vinyl formamide, research grade sodium acetate, acetic acid, O-(carboxymethyl) hydroxylamine hemihydrochloride (OCMH), and D₂O were purchased from Sigma. Hyaluronic acid, with an average molecular weight of 31 kD was purchased from Lifecore. Amino acids were purchased from Peptides International. Analytical grade acetonitrile and synthesis grade trifluoro acetic acid (TFA) were purchased from Fisher Scientific. Peptides and poly-*N*-vinyl formamide (PNVF) were synthesized by the laboratory. Water was provided by a Labconco Water PRO PS ultrapure water purification unit.

2.3 Methods

Peptide Synthesis. Aminoxy peptides were synthesized using 9-fluorenylmethyloxycarbonyl-protected amino acid chemistry on polyethylene glycol-polystyrene resins. The peptides synthesized were *aminoxy-LABL* (*aminoxy-ITDGEATDSG*, *Ao-LABL*), a cell-adhesion molecule antagonist,⁽¹⁴⁾ and *aminoxy-proteolipid peptide (PLP)* (*aminoxy-HSLGKWLGHPDKF*, *Ao-PLP*), a known antigen epitope in multiple sclerosis. Peptides were deprotected, cleaved from resin, and isolated by precipitation in ether. Purification was completed using preparatory high performance liquid chromatography (HPLC) followed by lyophilization. Peptide purity was assessed using analytical HPLC and the identity of the synthesized peptide was confirmed by electrospray ionization mass spectrometry.

Reaction of Aminoxy Molecules to Monomer/Polymer. The reaction conditions were identical for all monomers and polymers used (*N*-acetyl glucosamine, glucuronic acid, PNVF and hyaluronic acid). The aminoxy-containing small molecule OCMH and peptide species were both tested. For small molecule monomers, 45 μ mol NAG (Mw 221, 10.07 mg) was mixed with 45 μ mol OCMH (Mw 109, 4.97 mg) in 5 mL acetate buffered (20 mM) saline solution pH 5.5. After addition of all reactive species the pH was measured and adjusted to 5.5 ± 0.1 . For poly-

mers and peptide reactions, 1.3 μMol polymer was dissolved into 20 mM acetate buffered saline (pH 5.5 ± 0.1). Once dissolved, 1.3 μMol aminooxy-peptide was added to the solution. When more than one peptide species was added, 0.65 μMol of each peptide was weighed out separately then both were added simultaneously. After addition of the aminooxy species, the reaction solution pH was adjusted to pH 5.5 ± 0.1 . The solution was mixed for 16 hr at room temperature. After 16 hrs the samples were frozen at $-70\text{ }^{\circ}\text{C}$ and lyophilized. For kinetic experiments, samples were taken from the reaction vessel at predetermined time points and analyzed immediately. For peptide conjugates the reaction products were purified by dialysis to remove excess free peptide, and lyophilized. Exact procedure for reaction can be found in supplemental materials.

Mass Spectroscopy. Masses of conjugates and of synthesized peptides were determined by electrospray ionization mass spectroscopy by using a waters LCT premier ESI mass spectrometer running MassLynx software.

Fourier Transform Infrared Spectroscopy. Changes in bonding environments during reaction were monitored using a Bruker Tensor 27 FTIR spectrometer equipped with a ZnSe attenuated total reflectance (ATR) plate (Pike Technologies). Fourier transform infrared (FTIR) spectra were collected at room temperature ($25\text{ }^{\circ}\text{C}$). Data were collected over 256 composite scans with a resolution of 4 cm^{-1} . The samples were analyzed in 20 mM acetate buffered saline at a concentration of 3 mg/mL. Spectra from OCMH in solution were subtracted using the OPUS spectroscopy software and data were further analyzed using GRAMS/AI (Galactic, Inc.).

Nuclear Magnetic Resonance Spectroscopy. For structural analysis of the various monomers and conjugates, samples were dissolved in D_2O to a concentration of 10 mg/mL. ^1H and ^{13}C spectra were acquired on a Bruker 400MHz spectrometer at $25\text{ }^{\circ}\text{C}$.

Gel Permeation Chromatography. The change in molecular weight of hyaluronic acid conjugates was determined using a Viscotek GPC max VE 2001 GPC solvent/sample module, VE 3580 refractive index detector, and 270 Dual Detector with right angle light scattering. Samples

were separated by utilizing a tandem column setup of two Viscogel, GMPWxl grade, columns (Viscotek) at a flow rate of 1 ml/min and isocratic elution in water for 30 min.

High Performance Liquid Chromatography. Peptide was quantified by gradient reversed-phase HPLC (SHIMADZU) using a Vydac HPLC protein and peptide C18 column. The HPLC consisted of a SCL-20A SHIMADZU system controller, LC-10AT VP SHIMADZU liquid chromatograph, SIL-10A XL SHIMADZU auto-injector set at 75 μ L injection volume, DGU-14A SHIMADZU degasser, sample cooler, and SPD-10A SHIMADZU UV-vis detector (220 nm). The HPLC-UV system was controlled by a personal computer equipped with SHIMADZU class VP Software. Gradient elution was carried out at constant flow of 1 mL/min, from 100% A to 35% A (corresponding to 0% B to 65% B) for 50 min, followed by an isocratic elution at 75% B for 3 min. Mobile phase compositions were (A) acetonitrile-water (5:95) with 0.1% TFA and (B) acetonitrile-water 90:10, v/v) with 0.1% TFA. At the end of each analysis, the cartridge was re-equilibrated at initial conditions at 1 mL/min flow rate for 5 min with A.

2.4 Results and Discussion

Aminoxy chemistry presents an opportunity for glycoconjugation in a specific manner due to the preferential reactivity of the amino ester for certain carbonyl carbons. (2) Aminoxy reactivity to aldehydes and ketones is well known, (1, 3, 15-16) but reactivity to free amides (e.g. *N*-acetyl or *N*-formyl) has yet to be explored. It has been previously reported that hyaluronic acid (HA) modification with aldehydes confers aminoxy reactivity; (1, 6) however, the potential to react directly to unmodified *N*-acetyl sites on HA or other glycosaminoglycans (GAG) would have far reaching implications. In addition, conjugation to GAGs or inversely, the synthetic glycosylation of polypeptides, typically requires complicated reaction schemes. A single-step, aqueous glycoconjugation strategy would be useful.

Using O-(carboxymethyl) hydroxylamine (OCMH), the potential for an aminoxy reaction to the monomers of HA, glucuronic acid (GLU) and *N*-acetyl glucosamine (NAG), was probed.

Both of these groups display a carbonyl carbon; a carboxylic acid on glucuronic acid and an amide on *N*-acetyl glucosamine (Figure 1). Individual monomers were reacted with OCMH in an acetate buffered saline and the product was analyzed by mass spectroscopy. The spectrum for the reaction product between GLU and OCMH (Figure 2) showed the presence of the GLU ($M_w = 144.1$) and OCMH ($M_w = 91$), however, no reaction product was present. In the mass spectra for the reaction between NAG and OCMH, a peak at a mass of 317 Da was found in addition to the reactants themselves (Figure 3). This molecular mass was equivalent to the theoretical mass expected for aminooxy conjugation through the *N*-acetyl site of NAG, thus supporting the possibility of an *N*-oxime reaction scheme. It should be noted that in both mass spectra for GLU and NAG, there is a peak at 286 for GLU and at 285 for NAG in the stock material that also appears in the final product.

With the mass spectroscopy data suggesting a reaction was occurring, the products were analyzed to identify the groups involved in the reaction process. The NAG + OCMH product was analyzed by 1H (Figure 4) and ^{13}C (Figure 5) NMR. The 1H NMR data showed the appearance of new environments at ~2 ppm as a result of the methyl hydrogens in the OCMH backbone, and at 6.5 and 7.5 ppm due to the appearance of the proposed *N*-oxime bonding environments. The ring environment from 3-4 ppm shifted slightly, which could be due to interactions between NAG and the new OCMH side groups. ^{13}C NMR was used to identify the effected carbons in the reaction. The amide environment was indeed involved in the reaction as the amide carbon (~175 ppm) shifts to 150 ppm, indicative of the proposed *N*-oxime-bonded carbon. (17) Additionally, the carboxylic acid environment of unreacted OCMH appeared in the product spectra at 180 ppm along with the methyl carbons in the backbone of OCMH at 25 ppm. The NMR data supported the notion that the *N*-acetyl amide groups do confer aminooxy reactivity.

In addition to the NMR data, changes in bonding environments of the reactants were monitored throughout the course of the reaction. The experiment was conducted with the ami-

nooxy-reactive molecule OCMH in 10-fold excess and any changes in either GLU or NAG were monitored using FTIR over a 24 hour reaction period. For all FTIR spectra, the free OCMH in solution was subtracted resulting in the FTIR spectra showing only changes in NAG or GLU. When the reaction between GLU and OCMH was analyzed, the FTIR data showed no change in the bonding environment over the entire 24 hr period (Figure 6-A). When the reaction of NAG and OCMH was analyzed (Figure 6-B), the amide bonding environments at 1650 and 1550 cm^{-1} decreased throughout the course of the reaction. In addition to the disappearance of the amide bonding environments, two new bonding environments appeared; the carboxylic acid environment due to the addition of OCMH to NAG at 1700 cm^{-1} and an expected *N*-oxime environment at 1250 cm^{-1} . Thus, mass spectroscopy, NMR, and FTIR data demonstrated that a reaction is occurring between the amide carbon of NAG and the aminooxy of OCMH.

An additional control study was conducted to further evaluate aminooxy reactivity to free amides. In this study, polyacrylic acid (only carboxylic acid side groups) and poly-*N*-vinyl formamide (only *N*-formyl side groups) were probed for aminooxy reactivity. Polyacrylic acid exhibited no reactivity as expected (Supplementary Figure 1-A) while poly-*N*-vinyl formamide reacted with OCMH. A time course analysis using FTIR showed a decrease in amide peak at 1650 cm^{-1} and an increase in an *N*-oxime bond peak as the appearance of a shoulder at 1600 cm^{-1} (Supplementary Figure 1-B).

N-oxime chemistry was further probed by grafting an aminooxy reactive peptide to hyaluronic acid (HA). The peptides LABL and PLP were synthesized with a terminal aminooxy group to confer reactivity. The peptide molecular weights were confirmed by mass spectroscopy (Supplementary Figure II-A and Supplementary Figure II-B) with a purity >90% as determined by HPLC. In the first study, *Ao*-LABL was mixed with HA in acetate buffered saline. For reference, the number of reactive sites per mole of HA was calculated by dividing the mean molecular weight of HA by the monomer unit molecular weight (Table 1). After the designated reaction time, the product was extensively dialyzed to remove any unreacted free peptide. The conju-

gate product and the dialysate were lyophilized and the reaction efficiency was determined by reversed-phase HPLC. The mass of unreacted peptide in the dialysate was compared to the mass of peptide conjugated to the HA. Grafted *Ao-LABL* was hydrolyzed from the conjugate prior to analysis using buffer at pH 2 (Table 2). A reaction efficiency of 64% was achieved at 8 hours reaction time. By extending the reaction time from 8 hours to 16 hours and maintaining the buffer at 20 mM acetate, a reaction efficiency of ~90% was achieved (Table 2).

In addition to analyzing the peptide concentration hydrolyzed from the HA, the change in size of the conjugate product was also analyzed by GPC and compared to different molecular weights of HA (Figure 7). The conjugate product showed an increase in relative molecular weight as indicated by the shift to a smaller retention volume. The peak width remained relatively constant suggesting that the polydispersity of HA did not substantially change after conjugation. Thus, the peptide graft density may have been similar on each HA chain.

Next, the simultaneous conjugation of two aminooxy-peptides was investigated. Equal moles of *Ao-LABL* and *Ao-PLP* were added to HA and the reaction was carried out for 16 hours. After extensive purification by dialysis and lyophilization of the product, the peptides were cleaved from HA and analyzed by HPLC to determine the mole percent of each peptide on the HA backbone. Both peptides were grafted to HA at nearly an equimolar ratio (Table 3).

The stability of the *N*-oxime bond between the peptide and HA polymer was also investigated by challenging the conjugate with different pH buffer conditions. Previous studies involving oxime bonds resulting from the reaction of aminooxy groups with aldehydes or ketones have shown that the oxime bond is labile to both acid- and base-catalyzed hydrolysis. The rate of hydrolysis was pH dependent at high and low pH; however, the rate becomes independent of pH between pH 5-8. (18-19) The stability of the synthesized HA-peptide conjugates was evaluated across a pH range of 2 – 7.5 by putting the dissolved conjugate into three different pH buffer conditions and measuring the peptide released into solution. The released peptide hydrolyzed from the HA backbone was quantified by HPLC over the course of 300 minutes. Con-

jugates at pH 5.5 and 7.5 reached an apparent equilibrium by 240 minutes with a total of 10% of peptide hydrolyzed from the conjugate. At pH 2, 100% of the peptide was hydrolyzed after only 60 minutes (Figure 8).

2.5 Conclusions

In this report, a single-step glycoconjugation in aqueous buffer was performed by reacting an aminooxy small molecule or peptide to the amide side chain of *N*-acetyl glucosamine or hyaluronic acid. In addition to the conjugation of a single aminooxy reactive molecule, it was demonstrated that two different peptides could be conjugated to hyaluronic acid in an equimolar ratio. This *N*-oxime chemistry establishes a simple and unique scheme for reacting available amides to aminooxy compounds, thus enabling simple strategies for glycoconjugation.

TABLES

Table 1: Molar concentration of amide sites per mole of HA.

Mean HA Mw (Da)	Monomer unit Mw (Da)	# amide sites per Mole of HA
31,000	417	74.3*

*Indicates the number of amide sites. For reference, there are an equal number of carboxylic acid sites.

Table 2: Mass balance of HA – *Ao-LABL* conjugate product as compared to standard control.

Sample	Area Under Curve	Total Area of Peaks
<i>Ao-LABL</i> Peptide	8799141	8799141
HA conjugate (8 hr)*	5633361	8774823
Dialysis Solution (8 hr)**	3141462	
HA conjugate (16 hr)*	8421520	8421520
Dialysis Solution (16 hr)**	Not detected	

*Peptide was first hydrolyzed from HA at pH 2

**Unreacted peptide in dialysate

Table 3: HPLC analysis of dual-peptide conjugate.

Peptide	Concentration (nMol)	mol %
<i>Ao-LABL</i>	650	54
<i>Ao-PLP</i>	550	46

FIGURES

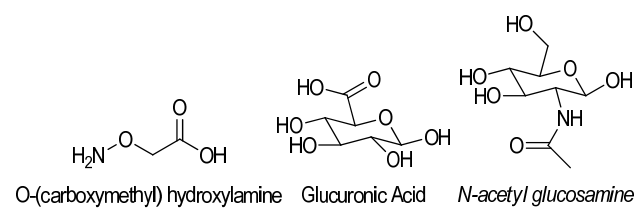


Figure 1: Structures of O-(carboxymethyl) hydroxylamine, glucuronic acid, and N-acetyl glucosamine

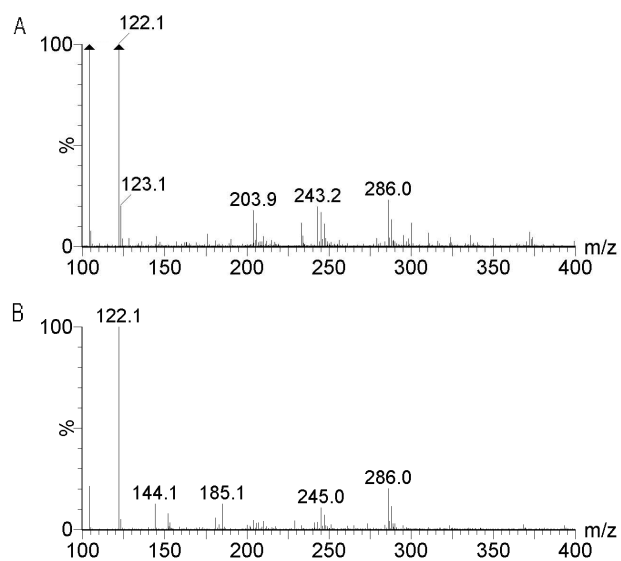


Figure 2: (A) ESI+ mass spectroscopy of GLU stock material. (B) ESI+ mass spectroscopy of the unpurified mixture of glucuronic acid and OCMH showing the absence of any product peak.

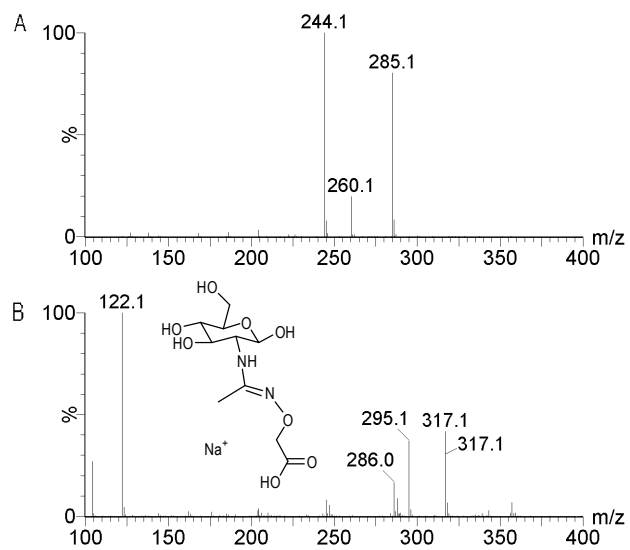


Figure 3: (A) ESI+ mass spectroscopy of NAG stock material. (B) ESI+ mass spectroscopy of the unpurified reaction product between NAG and OCMH showing the product peak at 295 and product plus Na⁺ at 317.

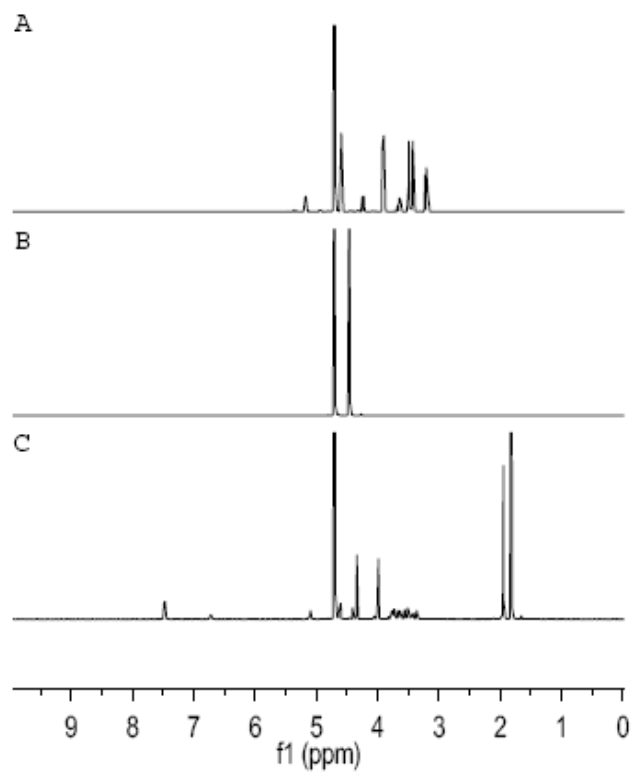


Figure 4: ¹H NMR spectrum showed expected changes from (A) NAG and (B) OCMH to (C) reaction product of NAG monomer with OCMH. Product spectra showed the appearance of peaks at ~6.5 and 7.5 ppm corresponding to the proposed *N*-oxime bonding environment.

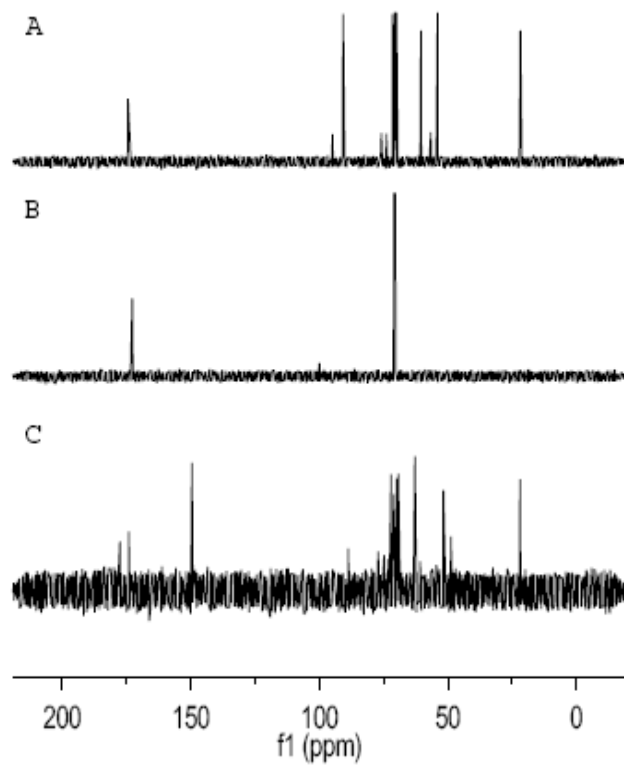


Figure 5: ¹³C NMR spectrum showed expected changes from (A) NAG monomer and (B) OCMH to (C) reaction product of NAG monomer and OCMH. The product spectra showed that the amide carbon peak (~175 ppm) shifted to ~150 ppm indicative of the proposed *N*-oxime bonding environment.

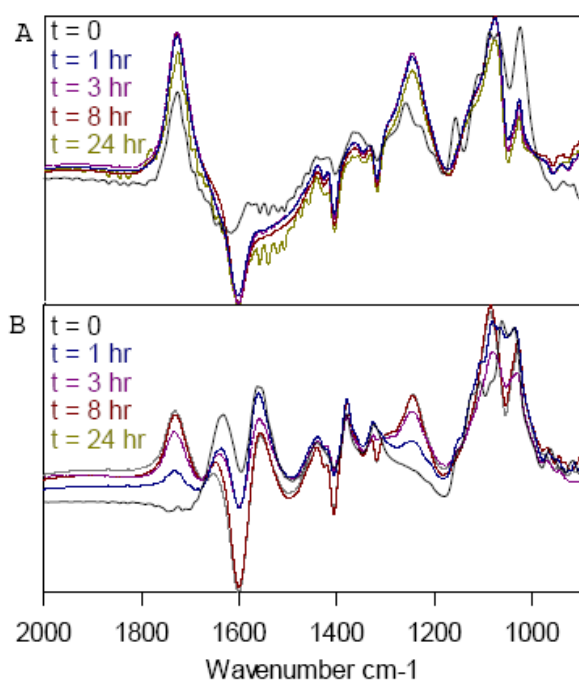


Figure 6: (A) FTIR spectra showed no change over time in glucuronic acid mixed with OCMH. (B) FTIR spectra showed changes in bonding environments for NAG reacted with OCMH. The decrease in absorbance at 1650 and 1550 cm^{-1} and the increase in absorbance at ~1750 and 1250 cm^{-1} over time are indicative of the loss of the amide environment and the appearance of carboxylic acid and proposed *N*-oxime environments due to the reaction of NAG with OCMH.

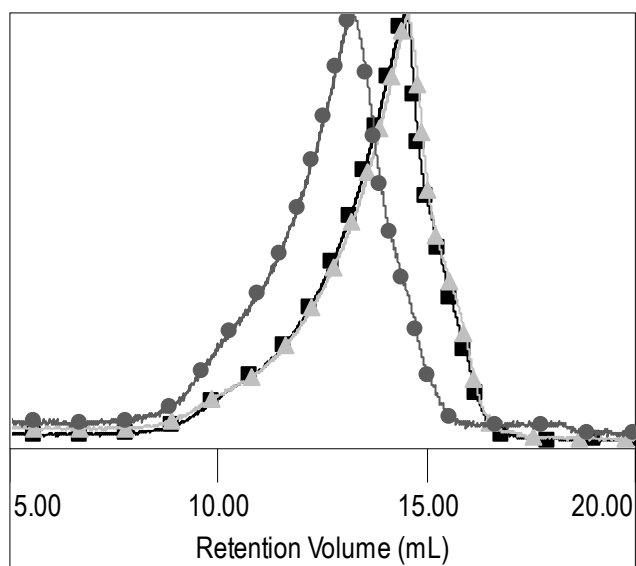


Figure 7: GPC refractive index chromatograms showed the increase in molecular weight as indicated by smaller retention volumes for hyaluronic acid with grafted Ao-peptides (circles) compared to 17 kD hyaluronic acid (triangles) and 31 kD hyaluronic acid (squares).

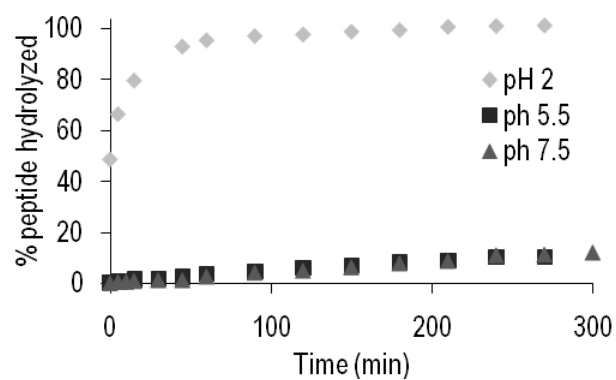
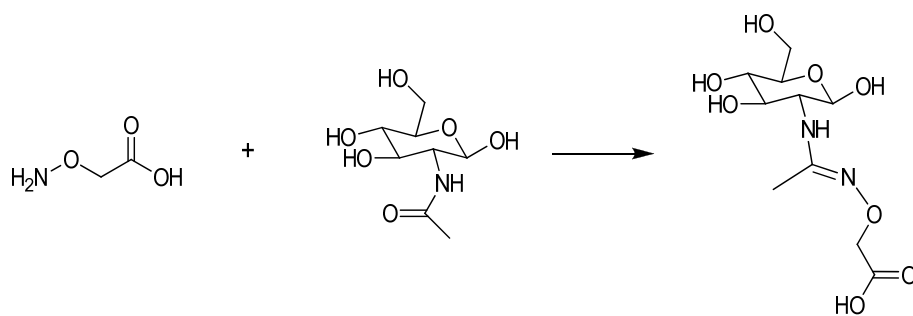


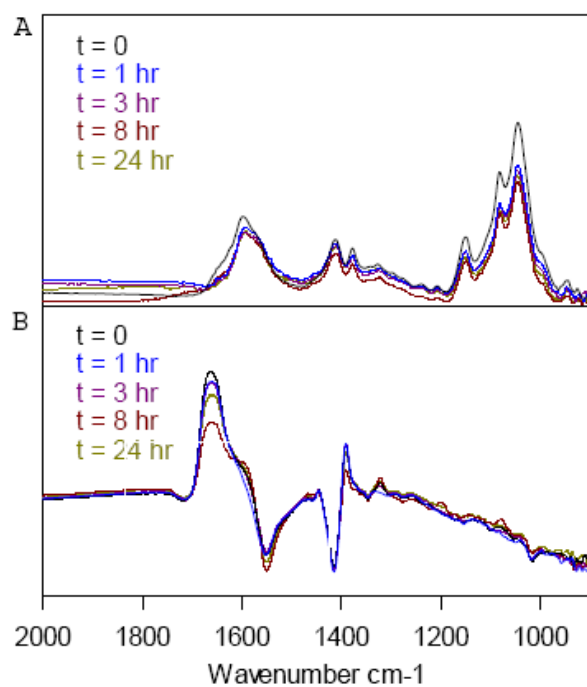
Figure 8: The release of Ao-LABL peptide from hyaluronic acid by hydrolysis of the *N*-oxime bond at three pH conditions. At pH 5.5 and 7.5, peptide concentration approached 10% after ~240 minutes while ~100% of the peptide was hydrolyzed from HA after 60 minutes at pH 2.

SCHEMES

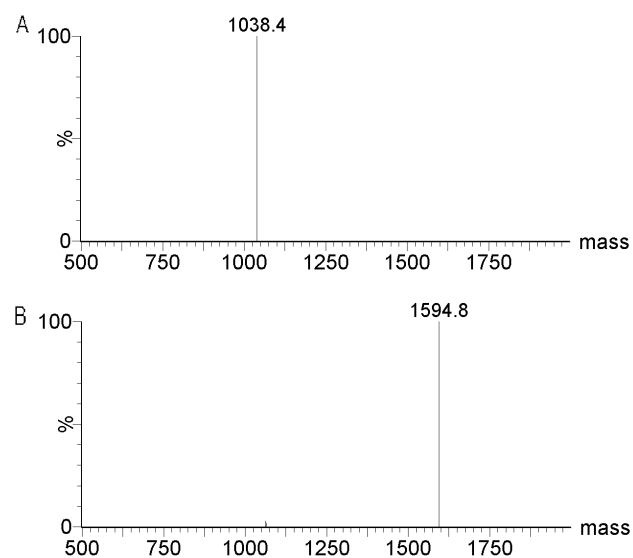


Scheme 1: The proposed reaction of aminooxy reactive OCMH with the amide of *N*-acetyl glucosamine.

SUPPLEMENTARY FIGURES



Supplementary Figure 1: (A) The FTIR spectra of a mixture of the PAA polymer (carboxylic acid side groups) with OCMH showed no change in bonding environments. (B) The FTIR spectra of the reaction of PNVF (amide side groups) with OCMH showed a decrease in the amide peak at 1650 cm^{-1} and an increase in the *N*-oxime bond peak as the appearance of a shoulder at 1600 cm^{-1} .



Supplementary Figure 2: (A) ESI+ mass spectroscopy of purified Ao-LABL peptide with the expected mass of 1038. (B) ESI+ mass spectroscopy of purified Ao-PLP peptide with the expected mass of 1594.

REFERENCES

1. Gajewiak J, Cai S, Shu XZ, Prestwich GD. Aminoxy Pluronics: Synthesis and Preparation of Glycosaminoglycan Adducts. *Biomacromolecules*. 2006;7(6):1781-9.
2. Heredia KL, Tolstyka ZP, Maynard HD. Aminoxy End-Functionalized Polymers Synthesized by ATRP for Chemoselective Conjugation to Proteins. *Macromolecules*. 2007;40(14):4772-9.
3. Hwang J, Li RC, Maynard HD. Well-defined polymers with activated ester and protected aldehyde side chains for bio-functionalization. *J Control Release*. 2007;122(3):279-86.
4. Jencks WP. Studies on the Mechanism of Oxime and Semicarbazone Formation1. *Journal of the American Chemical Society*. 1959;81(2):475-81.
5. Kalia J, Raines Ronald T. Hydrolytic Stability of Hydrazones and Oximes13. *Angewandte Chemie*. 2008;120(39):7633-6.
6. Boltje TJ, Buskas T, Boons G-J. Opportunities and challenges in synthetic oligosaccharide and glycoconjugate research. *Nat Chem*. 2009;1(8):611-22.
7. Zvilichovsky G, editor. *PATAT'S Chemistry of Functional Groups; Hydroxylamines, Oximes and Hydroxamic acids*: John Wiley & Sons Ltd; 2010.
8. Diezmann F, Eberhard H, Seitz O. Native chemical ligation in the synthesis of internally modified oligonucleotide-peptide conjugates. *Peptide Science*. 2010;94(4):397-404.
9. Marc A. Gauthier, Harm-Anton Klok. *ChemInform Abstract: Peptide/Protein - Polymer Conjugates: Synthetic Strategies and Design Concepts*. *ChemInform*. 2008;39(39).
10. Raines JKaRT. *Advances in Bioconjugation*. *Curr Org Chem*. 2010;14(2):138-47. PMID: PMC2901115.
11. Guo Y, Fujiwara K, Uneyama K. A Novel Route to Dipeptides via Noncondensation of Amino Acids: 2-Aminoperfluoropropene as a Synthon for Trifluoroalanine Dipeptides. *Organic Letters*. 2006;8(5):827-9.
12. Shimaoka H, Kuramoto H, Furukawa J-i, Miura Y, Kurogochi M, Kita Y, et al. One-Pot Solid-Phase Glycoblotting and Probing by Transoximization for High-Throughput Glycomics and Glycoproteomics. *Chemistry – A European Journal*. 2007;13(6):1664-73.
13. Fraser JR, Laurent TC, Laurent UB. Hyaluronan: its nature, distribution, functions and turnover. *J Intern Med*. 1997;242(1):27-33.
14. Yusuf-Makagiansar H, Makagiansar IT, Hu Y, Siahaan TJ. Synergistic inhibitory activity of [alpha]- and [beta]-LFA-1 peptides on LFA-1/ICAM-1 interaction. *Peptides*. 2001;22(12):1955-62.
15. Mikkel B. Thygesen KKS, Emiliano Cló and Knud J. Jensen. Direct chemoselective synthesis of glyconanoparticles from unprotected reducing glycans and glycopeptide aldehydes. *Chem Commun*. 2009:6367 - 9.
16. Namavari M, Cheng Z, Zhang R, De A, Levi J, Hoerner JK, et al. A Novel Method for Direct Site-Specific Radiolabeling of Peptides Using [18F]FDG. *Bioconjugate Chemistry*. 2009;20(3):432-6.
17. Hawkes GE, Herwig K, Roberts JD. Nuclear magnetic resonance spectroscopy. Use of carbon-13 spectra to establish configurations of oximes. *The Journal of Organic Chemistry*. 1974;39(8):1017-28.
18. Conant JB, Bartlett PD. A QUANTITATIVE STUDY OF SEMICARBAZONE FORMATION. *Journal of the American Chemical Society*. 1932;54(7):2881-99.
19. Kalia J, Raines RT. Hydrolytic Stability of Hydrazones and Oximes. *Angewandte Chemie International Edition*. 2008;47(39):7523-6.

Chapter 3

Evaluation of SAgA efficacy and effect of SAgA scaffold

3.1 Introduction

Autoimmune diseases are often propagated through professional antigen presenting cells (pAPCs) stimulating the clonal expansion of T-cells recognizing endogenous antigen. In the autoimmune disease multiple sclerosis (MS), activation of immune cells leads to attack on the central nervous system (CNS) resulting in neural degeneration. The majority of FDA-approved therapies focus on suppressing disease symptoms through inhibition of the immune inflammatory response, despite substantial side effects. (1) Newer therapies aim to return function after an attack, prevent new attacks, and prevent disability. (2) These approaches are common among many autoimmune disorders such as diabetes, rheumatoid arthritis, lupus, and asthma, but, they typically fail to address the underlying pathogenesis. (3) Therapies that specifically disarm the immune response induced by offending endogenous antigens are needed.

In MS, new therapeutic strategies have recently emerged. Clinical data for the monoclonal antibody (mAb) TY2SABRI® revealed that blocking integrin $\alpha 4\beta 1$ led to improvement in patients with MS. (4-7) Immune suppression (8) and risk of multiple serious side effects, (9) however, are still a concern. Ineffective disease treatment has led to a new class of “antigen-specific” therapeutics. (10) An FDA-approved MS therapy that utilizes this approach, Copaxone®, employs polymeric antigen in an effort to promote tolerance by inducing regulatory T-cells. (11-13) Although clinical enthusiasm is somewhat dampened by adverse events and questionable long term effectiveness, Copaxone® demonstrates that this form of antigen delivery can improve clinical outcomes.

Utilizing antigen to induce specific immune responses is not new. Vaccines commonly use adjuvanted antigen presented as repeating patterns adsorbed on surfaces to induce immune protection. (14-17) Alternatively, frequent low doses of soluble antigen have been used to induce tolerance. In both cases, the formulation and dose regimen are customized and underlying mechanisms of action are typically complex. Traditional formulations often focus on

the chemical induction of the immune response (e.g. adjuvanting to activate toll-like receptors). But, the physical context of antigen presentation is a critical driver of immune response as well. (18-19)

Beginning in 1976, Dintzis and others systematically studied a wide range of polymers with grafted 'haptens' (e.g. antigens) and developed a set of rules for inducing immune stimulation or tolerance. (20-21) This research demonstrated that, while molecular mass of the therapeutic did play an important role, the hapten valency was also critical in eliciting an immune response. Much like conserved sequences or patterns on pathogens that are recognized by the immune system, "Dintzis Rules" proposed that characteristics such as polymer size, solubility, and flexibility, as well as antigen valency, spacing and binding avidity are necessary to direct the immune response.

Other research has focused on the chemical context of antigen recognition. Surfaces displaying both grafted antigen and grafted cell-adhesion molecule achieve efficacy by interrupting the formation of the immunological synapse. (22-26) A "bi-functional peptide inhibitor" (BPI) synthesized by the fusion of an MS epitope peptide, PLP, and a cell-adhesion molecule inhibitor peptide (LABL) via a flexible linker of defined length has demonstrated efficacy in the EAE model. (27) While the mechanism behind its efficacy has not been elucidated, previous research showed that by binding ICAM-1 one could block T-cell adhesion to intestinal epithelial cell monolayers. (28) Building off of these results, BPI was designed to display antigen and cell-adhesion inhibitors simultaneously. These results led to the hypothesis that BPI could bind multiple cell signaling molecules simultaneously on the surface of the APC or T cells, thereby inhibiting immunological synapse formation.

These findings plus Dintzis work prompted rational design of nanomaterials that display multiple copies of antigen and that simultaneously inhibit cell-adhesion. Soluble Antigen Arrays (SAGAs) were synthesized by grafting a known MS antigen derived from proteolipid protein amino acids 139-151 (PLP) and, an ICAM-1 inhibitor (LABL) to hyaluronic acid (HA) via a novel

N-oxime chemistry (Chapter 2). Once efficacy was demonstrated, the effect of dose was explored. The physical properties (e.g. soluble HA polymer vs. PLGA nanoparticle) were also shown to play a vital role in efficacy. Thus, these multivalent polymer therapeutics displaying cell-adhesion inhibitors and/or antigen were explored as potential therapeutics in treating experimental autoimmune encephalomyelitis.

3.2 Materials and Methods

Materials. Hyaluronic acid (HA), with an average molecular weight of 31 kD was purchased from Lifecore. Analytical grade acetonitrile and synthesis grade trifluoro acetic acid (TFA) were purchased from Fisher Scientific. Research grade sodium acetate, acetic acid, and D₂O were purchased from Sigma. Water was provided by a Labconco Water PRO PS ultrapure water purification unit. Poly (DL-lactic-co-glycolic acid) (50:50) (PLGA; inherent viscosity of 1.05 dL/g, Mw ~101 kDa) was purchased from LACTEL Absorbable Polymers International (Pelham, AL, USA). Pluronic[®] F68 (Mw ~8.4 kD) and Pluronic[®] F108 (Mw ~14.6 kD) were obtained from BASF Corporation. Acetone, diethyl ether and 1X Tris/EDTA buffer solution (pH 8) were obtained from Fisher Scientific. D-mannitol, Dess-Martin periodianine, tert-butyl carbazate (TBC), trinitrobenzenesulfonic acid (TNBS), dichloromethane anhydrous (DCM) and Triton X-100 were purchased from Sigma-Aldrich.

Peptide Synthesis. Aminoxy peptides were synthesized using 9-fluorenylmethyloxycarbonyl-protected amino acid chemistry on polyethylene glycol-polystyrene resins. The peptides synthesized were aminoxy-LABL (aminoxy-ITDGEATDSG, *Ao-LABL*), a ligand of ICAM-1 and aminoxy-PLP (aminoxy-HSLGKWLGHDPKF, *Ao-PLP*), an antigen derived from proteolipid protein amino acids 139-151 (PLP₁₃₇₋₁₅₁). Peptides were deprotected, cleaved from resin, and isolated by precipitation in ether. Purification was completed using preparatory High Performance Liquid Chromatography (HPLC) followed by lyophilization. Peptide identity was verified and purity/content was assessed using Mass Spectroscopy and analytical HPLC. BPI,

which is a fusion of PLP and LABL, was synthesized and purified as previously reported (HSLGKWLGHDPKF-AcGAcGAc-ITDGEATDSG).(29)

Reaction of Aminoxy Peptides to Polymers. HA was dissolved in 20 mM Acetate buffer (pH 5.5 ± 0.1 pH units) and aminoxy reactive peptide(s) added. When both LABL and PLP peptides were used, each was weighed separately, and then added simultaneously. After addition of the peptide(s), the reaction solution pH was adjusted back to pH 5.5 ± 0.1 pH units. Reaction solutions were stirred at 500 RPM using magnetic stir bars for ~ 16 hr. After the reaction, the soluble antigen array (SAgA) product was purified by extensive dialysis to remove any unreacted peptide, and then lyophilized.

Gel Permeation Chromatography. The relative molecular weight of the HA and of the SAgAs was estimated using a Viscotek GPC max VE 2001 GPC solvent/sample module, VE 3580 refractive index detector, and 270 Dual Detector with right angle light scattering. A tandem column setup of two Viscogel GMPWxl columns (Viscotek) was used at a flow rate of 1 mL/min with isocratic elution in water for 30 min.

Conversion of terminal hydroxyl groups to terminal aldehyde groups on Pluronic® F108.

To conjugate peptides to Pluronic® on PLGA nanoparticles an oxidizing reagent was used to convert hydroxyl groups on Pluronic®F108 (Pluronic®F108-OH) to aldehyde groups (Pluronic®F108-CHO). (30) One gram Pluronic®F108-OH was dissolved in 30 mL DCM. Subsequently, 58.1 mg Dess-Martin periodianine was added and reacted for 24 h at room temperature. The product was purified by precipitation in cold diethyl ether, followed by filtration. The obtained Pluronic®F108-CHO was verified by nuclear magnetic resonance spectroscopy ($^1\text{H-NMR}$). Deuterated chloroform (CDCl_3) was used to dissolve the samples. The conversion percentage was also determined. An excess amount of TBC was added to the Pluronic®F108-CHO solution as previously described and the amount of unreacted TBC was measured using TNBS solution. A UV/VIS Spectrophotometer (SpectraMax) operating at 334 nm was employed to quantify the colored mixture of TBC and TNBS (30-32).

Preparation of PLGA nanoparticles. A solvent displacement method was employed to prepare PLGA nanoparticles (NPs). (33-34) Briefly, PLGA (inherent viscosity 1.05 dL/g) was dissolved in acetone (15 mg/mL). A mixture of 1425 μ L of PLGA solution and 75 μ L 1X Tris/EDTA buffer solution was injected into 15 mL water containing 0.1% w/v Pluronic[®] using a syringe pump (10 mL/hr) while stirring (1000 rpm). Stirring was continued for 1.5 hours and then excess surfactant was removed by centrifugation (15,000 rpm, 15 min, 4°C) for 3 cycles, re-suspending in water between cycles. Using a sonication bath (Branson 2510 ultrasonic cleaner). A 25:75 Pluronic[®] (CHO:OH) ratio was used for fabrication of NPs with conjugated PLP (NP-Array_{PLP}), LABL (NP-Array_{LABL}), or both (NP-Array_{LABL-PLP}). The 0:100 Pluronic[®] (CHO:OH) ratio was used as the control (NP-Blank) without any peptide conjugation.

Conjugation of Peptides to PLGA nanoparticles. Stock solutions of 2 mg/mL of PLP and LABL peptides were separately prepared. To prepare the NP-Array_{PLP}, 4.0 mL of PLP stock was added to 102.3 mg NPs in 3.52 mL of water. For NP-Array_{LABL} preparation, 2.6 mL of LABL stock was added to 112.5 mg NPs in 3.2 mL of water. Finally, to prepare the NP-Array_{LABL-PLP}, 3.6 mL of PLP stock and 2.34 mL of LABL stock were added to 227.84 mg NPs in 2.844 mL water. The volume of each nanoparticle sample was increased to 50 mL using ddH₂O. The volume of NP-Blank sample was also increased up to 50 mL as well (227.84 mg NPs). The samples reacted overnight and were purified by centrifugation (15,000 rpm, 15 min, 4°C) for 3 cycles, resuspending in water between cycles.

Dynamic Light Scattering. Particle size was measured using a ZetaPALS dynamic light scattering instrument (Brookhaven Instrument Corporation).

High Performance Liquid Chromatography. Quantification of free peptide post reaction was accomplished by gradient reversed phase HPLC (SHIMADZU) using a Vydac HPLC protein and peptide C18 column. HPLC system was composed of an SCL-20A SHIMADZU system controller, LC-10AT VP SHIMADZU liquid chromatograph, SIL-10A XL SHIMADZU auto-injector set at 75 μ L injection volume, DGU-14A SHIMADZU degasser, sample cooler, and SPD-10A

SHIMADZU UV-vis detector (220 nm). A personal computer equipped with SHIMADZU class VP software controlled the HPLC-UV system. Gradient elution was conducted at constant flow of 1 mL/min, from 100% A to 35% A (corresponding to 0% B to 65% B) over 50 min, followed by an isocratic elution at 75% B for 3 min. Mobile phase compositions were (A) acetonitrile-water (5:95) with 0.1% TFA and (B) acetonitrile-water (90:10, v/v) with 0.1% TFA. At the completion of each analysis, the cartridge was equilibrated at initial conditions at 1 mL/min flow rate for 5 min with A.

Calculation of Peptide density on the surface of NPs. Peptide surface density was calculated by subtracting the amount of peptide recovered after conjugation from the amount of peptide added to the NP suspension. This value was then divided by the total surface area assuming a normal Gaussian particle size distribution and using a particle density of 1.34 g/cm³. NP-Blank suspension was used as a negative control. PLP and LABL at molar ratios of 100:0, 50:50, and 0:100 were added to the NP-Blank and peptide adsorption was quantified as an additional control. Peptide adsorption to blank particles or plastic was negligible.

Induction of EAE and Therapeutic Study. SJL/J (H-2s) female mice, 4 – 6 weeks old, were purchased from The Jackson Laboratory and housed under specified, pathogen-free conditions at The University of Kansas. All protocols involving live mice were approved by the Institutional Animal Care and Use Committee. Mice were immunized subcutaneously (s.c) with 200 µg of PLP_{139–151} in a 0.2 mL emulsion composed of equal volumes of phosphate-buffered saline (PBS) and complete Freund's adjuvant (CFA) containing killed *Mycobacterium tuberculosis* strain H37RA (final concentration of 4 mg/mL; Difco). The PLP_{139–151}/CFA was administered to regions above the shoulders and the flanks (total of four sites; 50 µL at each injection site). In addition, 200 ng/100 µL of pertussis toxin (List Biological Laboratories Inc.) was injected intraperitoneally (i.p.) on the day of immunization (day 0) and 2 days post-immunization. The mice received s.c. injections of each sample, equivalent to 100 nMol PLP /100 µL, on days 4, 7, 10. All NP samples were sonicated to disperse NPs before injection. For HA samples and controls, 100 µL

of each vehicle was injected. For NP vehicles, 400 μ L solution was used to assure suspension stability. Disease progression was evaluated blindly by the same observer using clinical scoring as follows: 0, no clinical signs of the disease; 1, tail weakness or limp tail; 2, paraparesis (weakness or incomplete paralysis of one or two hind limbs); 3, paraplegia (complete paralysis of two hind limbs); 4, paraplegia with forelimb weakness or paralysis; and 5, moribund (mice were euthanized if they were found to be moribund). Body weight was also measured daily.

Statistical Analysis

Statistical differences were determined by comparing treated groups to the negative control (PBS) for clinical disease score and body weight. A one-way analysis of variance (ANOVA) followed by Fisher's least significant difference was applied to these data. All analyses were performed using GraphPad Software (GraphPad Software Inc.).

3.3 Results

Characterization of polymeric Soluble Antigen Arrays. Gel permeation chromatography (GPC) and HPLC were employed to observe any change in retention time resulting from the presence of peptides grafted to the HA. When analyzed by GPC, the product showed a decrease in retention time suggesting an increase in molecular weight relative to the HA (Figure 1). To quantify the amount of peptide grafted to the polymer, the product retentate and dialysate (containing unreacted peptide) were analyzed by HPLC after extensive dialysis. The product retentate was incubated at room temperature in pH 2 mobile phase buffer. At this pH, the *N*-oxime bond is rapidly hydrolyzed, thus allowing quantification of the peptide released from the product. Typical chromatograms showed the presence of the *Ao-LABL* peptide, the *Ao-PLP* peptide, or both (Figure 2-A). The dialysate showed no peaks. Any unreacted peptide was below the limit of detection of the HPLC (Figure 2-B). A 1:1 ratio of the peptides was achieved. The apparent difference in peak intensities was primarily due to the different absorption

coefficients of these peptides. Data for all the SAgA types suggested highly efficient grafting (Table 1).

Conversion of terminal hydroxyl groups to terminal aldehyde groups on Pluronic® F108.

The hydroxyl groups of Pluronic® were converted to aldehyde groups in order to utilize Pluronic® for conjugation to the terminal aminooxy of the PLP and LABL peptides. Pluronic® F108-CHO with aldehyde groups were prepared by the Dess-Martin oxidation reaction. To confirm conversion, ¹H NMR spectra from before and after the reaction were compared. After conversion, the signal corresponding to the aldehyde group ($\delta=9.75$) appeared which confirmed the conversion of hydroxyl groups to aldehyde groups (Supplementary Figure I). (30) The yield of the conversion was also determined to be 74.0% via a colorimetric TBC/TNBS assay. (31-32)

Characterization of NP-Arrays. Reversed phase HPLC was used to indirectly determine the amount of peptide conjugated to NPs. NPs were centrifuged from solution and the amount of unreacted peptide was quantified from the supernatant. Blank NPs and empty vials were used as controls to ensure that peptide was not being adsorbed to surfaces non-specifically. The peptide density on the surface of NPs was calculated based on the total NP surface area, assuming a normal Gaussian particle size distribution (Table 2). The NP-Array_{LABL-PLP} had a 1.1:1 ratio of LABL:PLP peptide on the surface. Light scattering data showed that all NP-Arrays showed similar size both before and after peptides were conjugated to the surface (Table 2). For the nanoparticles displaying only one peptide, the NP-Array_{PLP} had a similar surface density as the NP-Array_{LABL} (Table 1). The difference was not significant.

Suppression of EAE by Arrays. The SAgAs and NP-Arrays were evaluated in an EAE model induced in SJL/J mice. The *in vivo* study designs are outlined in Table 3. The disease onset usually occurs around day 8 and progresses to remission around day 20. Eight – 12 days after immunization, the mice showed disease signs, such as weakness, paralysis of their tail and limbs, and loss of body weight. Subcutaneous injections of each sample were given on days 4, 7, 10. SAgA_{LABL-PLP} inhibited the progression of EAE more effectively ($p<0.05$, day 17) than the

28 kDa HA which was used as the SAgA backbone (Figure 3). The mice in the SAgA_{LABL-PLP} treatment group had very low clinical scores throughout the study (Figure 3-A) and scores were significantly lower (at the peak of the disease; days 11–17) than those of groups treated with PBS. The mice treated with SAgA_{LABL-PLP} also had significantly better maintenance of body weight (Figure 3-B) compared to the negative control PBS group (days 12 – 17). In addition, 50% of the mice receiving the SAgA_{LABL-PLP} treatment never developed EAE during the course of study. Mice that showed few symptoms also exhibited a delay in disease onset (Figure 3-C). It should be noted that the HA polymer was administered at three times the molar concentration of HA in the SAgA_{LABL-PLP}. Previously, a similar molecular weight of HA was shown to suppress disease by activating toll-like receptors or increasing Th2 response (35-37), thus some therapeutic efficacy was expected for HA.

Once the efficacy of the SAgA_{LABL-PLP} was confirmed, the effect of SAgA_{LABL-PLP} dose was evaluated and compared to the positive control PLP-BPI. The BPI molecule was composed of three portions: the EAE antigen peptide (PLP) and the ICAM-1 inhibitor (LABL) separated by a spacer (see methods). Clinical results for BPI were consistent with previously published data. (27, 29, 38-39) The effect of SAgA_{LABL-PLP} dose was evaluated by increasing the concentration to 200 nM and 400 nM as defined by the molar quantity of PLP antigen administered. Clinical scores suggested that increasing the SAgA_{LABL-PLP} dose to 200 nM PLP reduced disease score ($p < 0.05$, day 15, Figure 4-A). Further increasing the concentration to 400 nM PLP gave results similar to the 200 nM dose as no significant difference was seen between dose levels. These results were corroborated by the weight loss in each treatment group, which showed similar trending (Figure 4-B).

The role of scaffold was investigated by replacing the hyaluronic acid polymer backbone with a PLGA-Pluronic® nanoparticle. The LABL and PLP peptides were grafted to the nanoparticles by reacting the aminooxy peptides to the particle surface. These particles were then delivered as a suspension with the dose of PLP at 100 nMol. The clinical scoring results

showed both the soluble polymer SAgA_{LABL-PLP} and colloidal NP-Array_{LABL-PLP} provided disease suppression (Figure 5-A), however, the NP-Array_{LABL-PLP} had a quicker onset and high incidence of disease when compared to the SAgA_{LABL-PLP} (Figure 5-C). Animal weight data indicated that the SAgA_{LABL-PLP} and NP-Array_{LABL-PLP} maintained animal body weight similarly throughout the study (Figure 5-B).

The effect of multivalent display of only antigen or only the cell-adhesion inhibitor was also investigated by conjugating either PLP peptide or LABL peptide to the HA polymer or to the NPs. As an additional control, a mix of free LABL and PLP peptides was tested. Clinical scores suggested that the multivalent LABL treatments (SAgA_{LABL} and NP-Array_{LABL}) exacerbated disease with data trending higher than that of the PBS control. Conversely, the multivalent PLP treatments (SAgA_{PLP} and NP-Array_{PLP}) showed trending similar to or slightly lower than the PBS control (Figure 6-A). Statistical analysis of these results, however, did not demonstrate statistical significance for either treatment. The weight loss results corroborated scoring data for both the multivalent LABL and multivalent PLP treatments (Figure 6-B). A mixture of free peptides (PLP and LABL) matched the PBS control indicating no clinical benefit (Figure 7). An outline of all results and statistical significance compared to negative the PBS control are summarized in Table 4.

3.4 Discussion

In multiple sclerosis, destruction of myelin in the central nervous system is propagated by CD4⁺ T cells. Activation of this subpopulation of T cells involves the formation of the immunological synapse at the interface between professional antigen presenting cells (pAPCs) and T cells. Multiple therapeutic approaches aim to disrupt antigen recognition or immune cell adhesion as discrete strategies. Modulation of immune response via peptide constructs has been the focus of much research in areas such as altered peptide ligands (APL), (40-43) splenocytes coupled with myelin basic protein (MBP)- or PLP- derived peptides, (44-45) and a

soluble MHCPLP_{139–151} construct. (46) The FDA-approved synthetic copolymer glatiramer acetate, marketed as Copaxone® contains four amino acids of MBP. It is reported to generate a Th2 response and/or induce tolerance (T_{reg}) as an APL. (47-48) Alternatively, therapies interrupting cell-adhesion include anti-CD28 Fab, (49) anti-CD40L antibody, (50) and the FDA-approved natalizumab marketed as TYSABRI®, an anti- α_4 integrin antibody. (51) By impeding cell-adhesion or co stimulation, these therapies can prevent lymphocyte recruitment or communication with pAPCs.

Combining these molecular strategies, prior research demonstrated a “bifunctional-peptide inhibitor” could suppress T-cell activation. (27, 38-39) It was hypothesized that efficacy was achieved by inhibiting the immunological synapse formation during antigen presentation to naïve T cells. The soluble antigen arrays (SAGAs) developed here were designed as a multivalent version of this BPI molecule, which displays antigen (PLP) and the ICAM-1 inhibitor LABL explored here. The antigen and LABL were, therefore, grafted to either a soluble, flexible HA or to a PLGA-NP. For both the HA and PLGA-NP arrays, the peptides were grafted according to the density and valency guidelines provided by “Dintzis Rules” (Table 1). (20, 52-57) According to these rules, one would expect a more pronounced suppression of EAE symptoms for the small, flexible, SAGA.

Initial studies showed SAGAs provided significant suppression of disease compared to both PBS and HA controls. Studies demonstrated that there may be a dosing optimum to achieve maximum disease suppression. The grafting of antigen and cell-adhesion inhibitor ligands significantly increased the ability of HA; a known CD44 antagonist, to provide EAE disease suppression. Results here coincide well with what is reported in the literature. Kiessling and others have analyzed the role cell-surface receptors play in coordinating cellular responses. (58-59) Most importantly, they showed the effect was not additive when using a multivalent polymer displaying two separate signaling inhibitors. Rather, the clustering of multiple receptors could enhance sensitivity or induce unique cellular responses. In addition to Kiessling’s work,

development of BPI demonstrated that it was the fusion of the antigen and ICAM-1 ligand that provided the therapeutic efficacy. (27, 29, 38)

When the BPI and SAgA results were compared in this study, they were found to be equivalent. The results suggested that efficacy was achieved by the coincident presence of the antigen and the cell-adhesion inhibitor. This hypothesis was tested by delivering arrays displaying antigen or only cell-adhesion inhibitor. Both the HA and NP arrays displaying antigen provided little benefit. The cell-adhesion inhibitor arrays appeared to cause a slight exacerbation of the disease, though the difference was not significant. The data supports the hypothesis that to achieve disease suppression both antigen and cell-adhesion inhibitor ligand must be delivered together.

Lastly, the correlation between performance and nanomaterial type was evaluated by preparing arrays on either a flexible polymer scaffold or a more rigid nanoparticle scaffold. Mice that received the NP-Arrays were able to maintain body weight throughout the study; however, the NP-Arrays did not reduce clinical scores to the same extent as the SAgAs. This may be due to the post injection fate of each of the materials. The SAgAs demonstrated a high aqueous solubility, suggesting that the arrays may be able to drain away from the injection site and into lymphatic or systemic circulation. Conversely, the NP-Arrays were a rigid colloid and most likely persisted at the site of injection. This was evident by a nodule remaining at the injection site for the duration of the study, unlike the SAgAs where the nodule dissipated after a few days. The relative immobility of the NP-Arrays after injection may induce recruitment of immune cells to the injection site and alter immune response or create a decoy effect. Nanomaterial chemistry or differences in molecular recognition may also affect efficacy. Further studies are needed, however, differences in the clinical data for SAgAs and NP-Arrays suggested that the physical characteristics must play a role in the efficacy of the arrays as well.

3.5 Conclusions

SAGAs presenting a disease-specific antigen (PLP) and a cell-adhesion molecule (ICAM-1) inhibitor grafted to hyaluronic acid provided significant suppression of EAE. Additionally, the presence of both the antigen and the cell-adhesion inhibitor was necessary to achieve suppression. The physical state of the array also played an important role in efficacy. When dosed with the relatively large NP-Array_{LABL-PLP} (~400 nm) the disease suppression was much less effective than the hyaluronic acid based SAgA_{LABL-PLP}. While it was demonstrated that both the polymer and nanoparticle materials displaying antigen and ICAM-1 inhibitors can improve disease scores, it was also shown that the physical characteristics of the material can alter the extent of the response.

3.6 References

1. Miller SD, Turley DM, Podojil JR. Antigen-specific tolerance strategies for the prevention and treatment of autoimmune disease. *Nat Rev Immunol*. 2007;7(9):665-77.
2. Compston A, Coles A. Multiple sclerosis. *The Lancet*. 2002;359(9313):1221-31.
3. Carter PH, Zhao Q. Clinically validated approaches to the treatment of autoimmune diseases. *Expert Opin Investig Drugs*. 2010;19(2):195-213.
4. Moriyama H, Yokono K, Amano K, Nagata M, Hasegawa Y, Okamoto N, et al. Induction of tolerance in murine autoimmune diabetes by transient blockade of leukocyte function-associated antigen-1/intercellular adhesion molecule-1 pathway. *J Immunol*. 1999;157:3737-43.
5. Kavanaugh AF, Davis LS, Jain RI, Nichols LA, Norris SH, Lipsky PE. A phase I/II open label study of the safety and efficacy of an anti-ICAM-1 (intercellular adhesion molecule-1; CD54) monoclonal antibody in early rheumatoid arthritis. *J Rheumatol*. 1996;23(8):1338-44.
6. Schulze-Koops H, Lipsky PE, Kavanaugh AF, Davis LS. Elevated Th1- or Th0-like cytokine mRNA in peripheral circulation of patients with rheumatoid arthritis. Modulation by treatment with anti-ICAM-1 correlates with clinical benefit. *J Immunol*. 1995;155(10):5029-37.
7. Steinman L. Blocking adhesion molecules as therapy for multiple sclerosis: natalizumab. *Nat Rev Drug Discov*. 2005;4(6):510-8.
8. Sheridan C. Tysabri raises alarm bells on drug class. *Nat Biotechnol*. 2005;23(4):397-8.
9. Langer-Gould A, Steinman L. Progressive multifocal leukoencephalopathy and multiple sclerosis: lessons from natalizumab. *Curr Neurol Neurosci Rep*. 2006;6(3):253-8.
10. Dolgin E. The inverse of immunity. *Nat Med*. 2010;16(7):740-3.
11. Aharoni R, Teitelbaum D, Leitner O, Meshorer A, Sela M, Arnon R. Specific Th2 cells accumulate in the central nervous system of mice protected against experimental autoimmune encephalomyelitis by copolymer 1. *Proc Natl Acad Sci U S A*. 2000;97(21):11472-7.
12. Senti G, Prinz Vavricka BM, Erdmann I, Diaz MI, Markus R, McCormack SJ, et al. Intralymphatic allergen administration renders specific immunotherapy faster and safer: a randomized controlled trial. *Proc Natl Acad Sci U S A*. 2008;105(46):17908-12.
13. Steinman L, Conlon P. Antigen specific immunotherapy of multiple sclerosis. *J Clin Immunol*. 2001;21(2):93-8.
14. Kool M, Petrilli V, De Smedt T, Rolaz A, Hammad H, van Nimwegen M, et al. Cutting edge: alum adjuvant stimulates inflammatory dendritic cells through activation of the NALP3 inflammasome. *J Immunol*. 2008;181(6):3755-9.
15. Ahmed N, Gottschalk S. How to design effective vaccines: lessons from an old success story. *Expert Rev Vaccines*. 2009;8(5):543-6.
16. Rolland JM, Gardner LM, O'Hehir RE. Allergen-related approaches to immunotherapy. *Pharmacol Ther*. 2009;121(3):273-84.
17. Lisak RP, Zweiman B, Blanchard N, Rorke LB. Effect of treatment with Copolymer 1 (Cop-1) on the in vivo and in vitro manifestations of experimental allergic encephalomyelitis (EAE). *J Neurol Sci*. 1983;62(1-3):281-93.
18. Dustin ML. The cellular context of T cell signaling. *Immunity*. 2009;30(4):482-92.
19. Sant AJ, Chaves FA, Jenks SA, Richards KA, Menges P, Weaver JM, et al. The relationship between immunodominance, DM editing, and the kinetic stability of MHC class II:peptide complexes. *Immunol Rev*. 2005;207:261-78.
20. Dintzis HM, Dintzis RZ, Vogelstein B. Molecular determinants of immunogenicity: the immunon model of immune response. *Proc Natl Acad Sci U S A*. 1976;73(10):3671-5. PMID: 431180.
21. Dixon FJ. *Advances in Immunology*. San Diego: Academic Press, Inc.; 1992.
22. Mossman KD, Campi G, Groves JT, Dustin ML. Altered TCR signaling from geometrically repatterned immunological synapses. *Science*. 2005;310(5751):1191-3.

23. Hartman NC, Nye JA, Groves JT. Cluster size regulates protein sorting in the immunological synapse. *Proc Natl Acad Sci U S A*. 2009;106(31):12729-34.
24. Dustin ML. The immunological synapse. *Arthritis Res*. 2002;4(Suppl 3):S119-25.
25. Dustin ML, Shaw AS. Costimulation: Building an immunological synapse. *Science*. 1999;283(5402):649-50.
26. Bromley SK, Iaboni A, Davis SJ, Whitty A, Green JM, Shaw AS, et al. The immunological synapse and CD28-CD80 interactions. *Nat Immunol*. 2001;2(12):1159-66.
27. Ridwan R, Kiptoo P, Kobayashi N, Weir S, Hughes M, Williams T, et al. Antigen-specific Suppression of Experimental Autoimmune Encephalomyelitis by a Novel Bifunctional Peptide Inhibitor: Structure Optimization and Pharmacokinetics. *J Pharmacol Exp Ther*. 2009.
28. Yusuf-Makagiansar H, Makagiansar IT, Hu Y, Siahaan TJ. Synergistic inhibitory activity of [alpha]- and [beta]-LFA-1 peptides on LFA-1/ICAM-1 interaction. *Peptides*. 2001;22(12):1955-62.
29. Naoki Kobayashi PK, Hitomi Kobayashi, Rahmawati Ridwan, Stefan Brocke, and Teruna J. Siahaan. Prophylactic and Therapeutic Suppression of Experimental Autoimmune Encephalomyelitis by a Novel Bifunctional Peptide Inhibitor. *Clinical Immunology*. 2008;129(1):69-79.
30. Yang T, Chen C, Chen M, Lai C, Liang H, Sung H. Shell-crosslinked Pluronic L121 micelles as a drug delivery vehicle. *Biomaterials*. 2007;28(4):725-34.
31. Bouhadir K, Hausman D, Mooney D. Synthesis of cross-linked poly (aldehyde guluronate) hydrogels. *Polymer*. 1999;40(12):3575-84.
32. Lee K, Bouhadir K, Mooney D. Degradation behavior of covalently cross-linked poly (aldehyde guluronate) hydrogels. *Macromolecules*. 2000;33(1):97-101.
33. Zhang N, Chittasupho C, Duangrat C, Siahaan TJ, Berkland C. PLGA Nanoparticle-Peptide Conjugate Effectively Targets Intercellular Cell-Adhesion Molecule-1. *Bioconjugate Chem*. 2008;19(1):145-52.
34. Chittasupho C, Xie SX, Baoum A, Yakovleva T, Siahaan TJ, Berkland CJ. ICAM-1 targeting of doxorubicin-loaded PLGA nanoparticles to lung epithelial cells. *European Journal of Pharmaceutical Sciences*. 2009.
35. Krejcova D PM, Safrankova B, Kubala L. The effect of different molecular weight hyaluronan on macrophage physiology. *Neuro Endocrinol Lett*. 2009;30((Suppl)):106-11.
36. Muto J YK, Taylor KR, Gallo RL. Engagement of CD44 by hyaluronan suppresses TLR4 signaling and the septic response to LPS *Mol Immunol*. 2009;47(2-3):449-56.
37. Tesar BM, Jiang D, Liang J, Palmer SM, Noble PW, Goldstein DR. The Role of Hyaluronan Degradation Products as Innate Alloimmune Agonists. *American Journal of Transplantation*. 2006;6(11):2622-35.
38. Kobayashi N, Kobayashi H, Gu L, Malefyt T, Siahaan TJ. Antigen-specific suppression of experimental autoimmune encephalomyelitis by a novel bifunctional peptide inhibitor. *J Pharmacol Exp Ther*. 2007;322(2):879-86.
39. Murray JS, Oney S, Page JE, Kratochvil-Stava A, Hu Y, Makagiansar IT, et al. Suppression of type 1 diabetes in NOD mice by bifunctional peptide inhibitor: modulation of the immunological synapse formation. *Chem Biol Drug Des*. 2007;70(3):227-36.
40. Kuchroo VK GJ, Kaul D, Ishioka G, Franco A, Sette A, Sobel RA, and Lees MB A single TCR antagonist peptide inhibits experimental allergic encephalomyelitis mediated by a diverse T cell repertoire. *J Immunol*. 1994;153:3326-36.
41. Stern JN IZ, Reddy J, Keskin DB, Fridkis-Hareli M, Kuchroo VK, and Strominger JL Peptide 15-mers of defined sequence that substitute for random amino acid copolymers in amelioration of experimental autoimmune encephalomyelitis. *Proc Natl Acad Sci U S A* 2005;102:1620-5.

42. Margot CD FM, and Evavold BD. Amelioration of established experimental autoimmune encephalomyelitis by an MHC anchor-substituted variant of proteolipid protein. *J Immunol.* 2005;174:3352–8.
43. DE SMaS. Reversal of acute experimental autoimmune encephalomyelitis and prevention of relapses by treatment with a myelin basic protein peptide analogue modified to form long-lived peptide-MHC complexes. *J Immunol.* 1995;155:2737–46.
44. Vanderlugt CL NK, Nikcevic KM, Eagar TN, Bluestone JA, and Miller SD. Pathologic role and temporal appearance of newly emerging autoepitopes in relapsing experimental autoimmune encephalomyelitis. *J Immunol.* 2000;164:670–8.
45. Smith CE ET, Strominger JL, and Miller SD. Differential induction of IgE-mediated anaphylaxis after soluble vs. cell-bound tolerogenic peptide therapy of autoimmune encephalomyelitis. *Proc Natl Acad Sci U S A.* 2005;102:9595–600.
46. Wang C GB, Kaler LJ, Yu X, Afentoulis ME, Burrows GG, Vandembark AA, Bourdette DN, and Offner H. Antigen-specific therapy promotes repair of Novel Peptide to Suppress Autoimmune Responses 885 myelin and axonal damage in established EAE. *J Neurochem.* 2006;98:1817–27.
47. Johnson KP BB, Cohen JA, Ford CC, Goldstein J, Lisak RP, Myers LW, Panitch HS, Rose JW, and Schiffer RB Copolymer 1 reduces relapse rate and improves disability in relapsing-remitting multiple sclerosis: results of a phase III multicenter, double-blind placebo-controlled trial. The Copolymer 1 Multiple Sclerosis Study Group. *Neurology.* 1995;45:1268–76.
48. Neuhaus O FC, Wekerle H, and Hohlfeld R. Mechanisms of action of glatiramer acetate in multiple sclerosis. *Neurology.* 2001;56:702–8.
49. Perrin PJ JC, Maldonado JH, Ratts RB, and Racke MK. Blockade of CD28 during in vitro activation of encephalitogenic T cells or after disease onset ameliorates experimental autoimmune encephalomyelitis. *J Immunol* 1999;163:1704–10.
50. Gerritse K LJ, Noelle RJ, Aruffo A, Ledbetter JA, Boersma WJ, and Claassen E. CD40-CD40 ligand interactions in experimental allergic encephalomyelitis and multiple sclerosis. *Proc Natl Acad Sci U S A.* 1996;93:2499–504.
51. Langer-Gould A AS, Green AJ, Bollen AW, and Pelletier D Progressive multifocal leukoencephalopathy in a patient treated with natalizumab. *N Engl J Med.* 2005;353:375–81.
52. Dintzis HM DR. Profound specific suppression by antigen of persistent IgM, IgG, and IgE antibody production. *Proc Natl Acad Sci U S A.* 1992;89(3):1113-7.
53. Reim JW SD, Watson DC, Dintzis RZ, Dintzis HM. Low molecular weight antigen arrays delete high affinity memory B cells without affecting specific T-cell help. *Mol Immunol* 1996;33(17-18):1377-88.
54. RZ D. Rational design of conjugate vaccines. *Pediatr Res.* 1992;32(4):376-85.
55. Symer DE DR, Diamond DJ, Dintzis HM. Inhibition or activation of human T cell receptor transfectants is controlled by defined, soluble antigen arrays. *J Exp Med.* 1992;176(5):1421-30.
56. Symer DE RJ, Dintzis RZ, Voss EW Jr, Dintzis HM. Durable elimination of high affinity, T cell-dependent antibodies by low molecular weight antigen arrays in vivo. *J Immunol.* 1995;155(12):5608-16.
57. Watson DC RJ, Dintzis HM. Suppression of the antibody response to a polymorphic peptide from the platelet alloantigen integrin beta3 with low molecular weight antigen arrays. *J Immunol.* 1996;156(7):2443-50.
58. Kiessling LL. Decoding Signals with Chemical Biology. *ACS Chemical Biology.* 2010;5(1):1-2.
59. Kiessling LL, Gestwicki JE, Strong LE. Synthetic Multivalent Ligands as Probes of Signal Transduction. *Angewandte Chemie International Edition.* 2006;45(15):2348-68.

TABLES

Table 1: Overview of peptide concentration and ratios on HA and NP scaffolds.

Sample	LABL Conc. (nMol)	PLP Conc. (nMol)	Final Ratio
SAgA _{LABL-PLP}	325	275	1.2:1
SAgA _{LABL}	462	-	n/a
SAgA _{PLP}	-	286	n/a
NP-Array _{LABL-PLP}	8.2	7.6	1.1:1
NP-Array _{LABL}	16.0	-	n/a
NP-Array _{PLP}	-	17.6	n/a

Table 2: Particle size for NP formulations before and after peptide conjugation.

Sample ID	Pluronic ratio (F108-CHO:F68-OH)	Particle Size (nm)*	
		After fabrication	After peptide conjugation
NP-Array _{LABL-PLP}	25:75	171±7.2	420±11
NP-Array _{LABL}	25:75	171±7.2	363±8.4
NP-Array _{PLP}	25:75	171±7.2	420±11
NP-Blank	0:100	158±1.9	419±12.1**


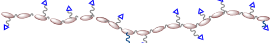
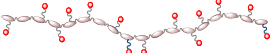


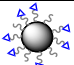
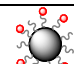
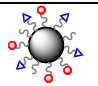
*Polydispersity values were < 0.1.55

**Samples handled analogously, but no peptide conjugation occurred

Table 3: Outline of individual *in vivo* studies conducted.

<i>Study I: Initial Efficacy Study</i>		
Group	Dose (nMol PLP/100 µL)	Description
Hyaluronic Acid		Polymer control
SAgA _{LABL-PLP}	100	LABL and PLP grafted to HA
PBS	0	Negative Control
<i>Study II: Dose Ranging Study</i>		
Group	Dose (nMol PLP/100 µL)	Description
SAgA _{LABL-PLP}	100	Low Dose
SAgA _{LABL-PLP}	200	Medium Dose
SAgA _{LABL-PLP}	400	High Dose
PBS	0	Negative Control
BPI	100	Positive Control
<i>Study III: Polymer vs. Nanoparticle Scaffold</i>		
Group	Dose (nMol PLP/100 µL)	Description
SAgA _{LABL-PLP}	200	HA graft LABL and PLP
SAgA _{LABL}	200 nMol LABL	HA graft LABL
SAgA _{PLP}	200	HA graft PLP
NP- Array _{LABL-PLP}	100	Nanoparticle graft LABL and PLP
NP- Array _{LABL}	100	Nanoparticle graft LABL
NP- Array _{PLP}	100	Nanoparticle graft PLP
PBS	0	Negative Control
BPI	100	Positive Control

Table 4: Summary of testing groups and clinical outcomes.

Treatment Group	PLP conc. (nMol)	Mw (Daltons)	Clinical Data Significance compared to PBS		Comments
			Score	% Weight loss	
Hyaluronic Acid Alone 	4.5 mg/mL**	28000	Days 11-14, p<0.01	Days 11-14, p<0.01	HA is a natural CD44 antagonist and provides minimal protection
SAgA _{LABL} 	100*	~70000	None	None	Grafting targeting moiety only causes disease exacerbation
SAgA _{PLP} 	100	~80000	None	None	Grafting antigen showed no effect
SAgA _{LABL-PLP} 	100	~80000	Days 11-17, p<0.01	Days 12-17, p<0.05	200 nMol may be optimal dose for SAgA _{LABL-PLP}
	200	~80000	Days 11-15, p<0.01	Days 11-15, p<0.01	
	400	~80000	Days 12-14, p<0.01	Days 12-14, p<0.05	
Blank NP 	100*	n/a	None	None	Nanoparticle based SAgA do not provide suppression of EAE
NP-Array _{LABL} 	100	n/a	Day 12, p<0.001	None	
NP-Array _{PLP} 	100	n/a	Day 12, p<0.001	Day 12, p<0.001	
NP-Array _{LABL-PLP} 	100	n/a	Day 12, p<0.001	Days 12-16, 18-22, p<0.01	

FIGURES:

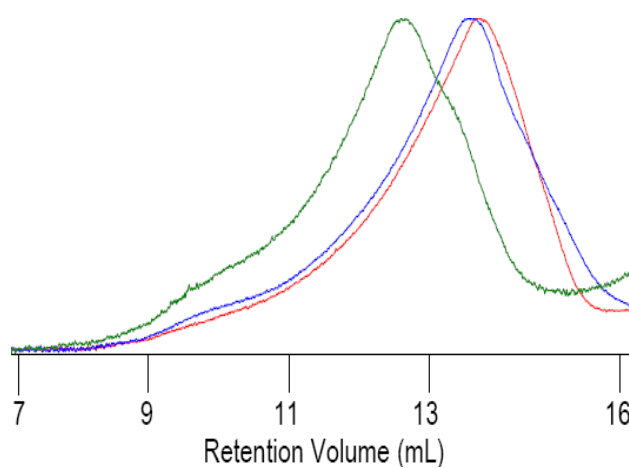


Figure 1: Refractive index GPC chromatogram demonstrating a decrease in retention time of the SAgA_{LABL-PLP} product (green line) as compared to 31 kDa (blue line) and 17 kDa (red line) HA standards indicating an increase in Mw.

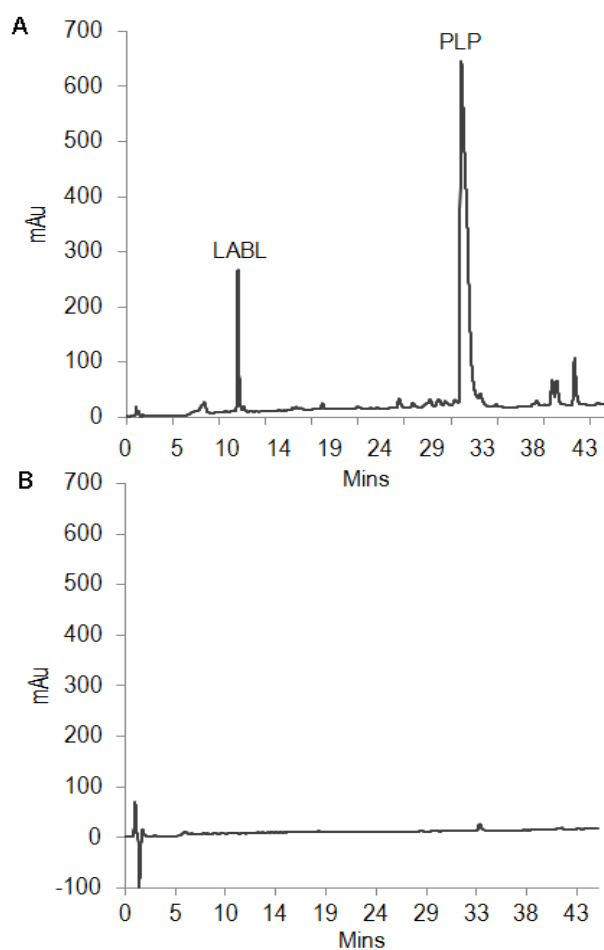


Figure 2: (A) Example HPLC chromatogram of peptides hydrolyzed from the conjugate product showing the presence of both the Ao-LABL and Ao-PLP peptides. (B) HPLC chromatogram of dialysate showing the absence of both the Ao-LABL and Ao-PLP peptides suggesting nearly all peptide was reacted to HA.

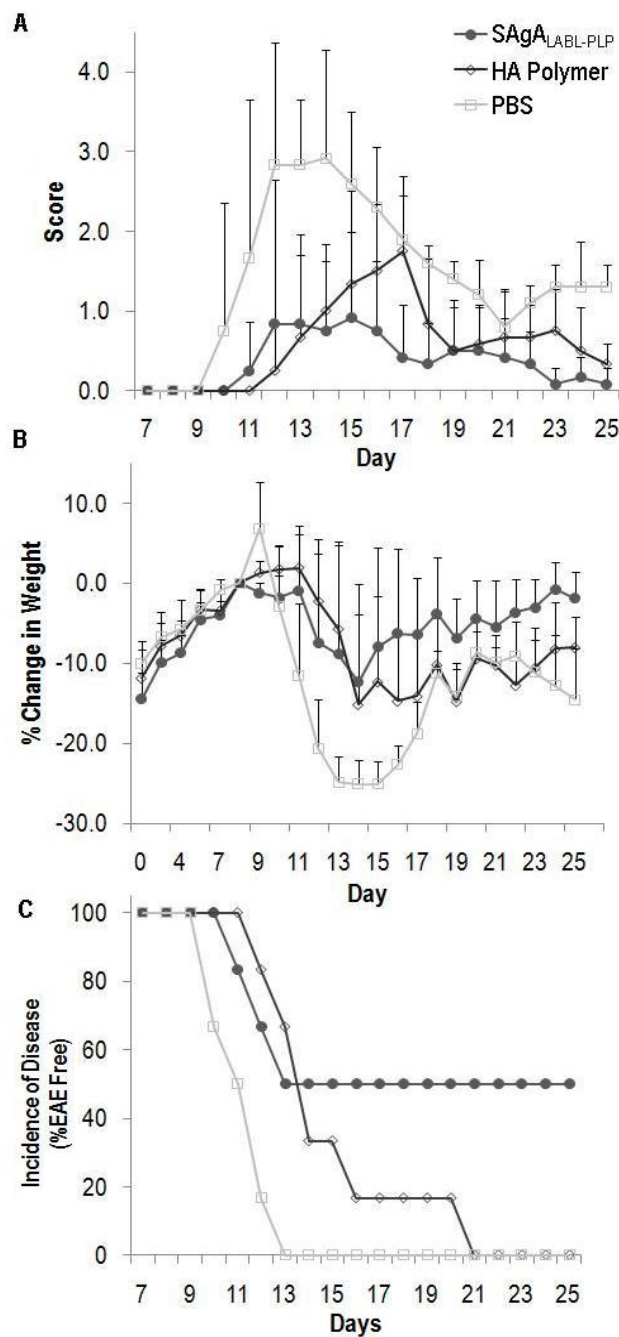


Figure 3: Comparison of clinical performance of SAgA_{LABL-PLP} to negative control (PBS) and polymer control (HA). The data show that SAgA_{LABL-PLP} performed significantly better than controls in (A) clinical disease score, (B) % change in body weight, and (C) incidence of disease. Differences that were statistically significant are summarized in Table 4.

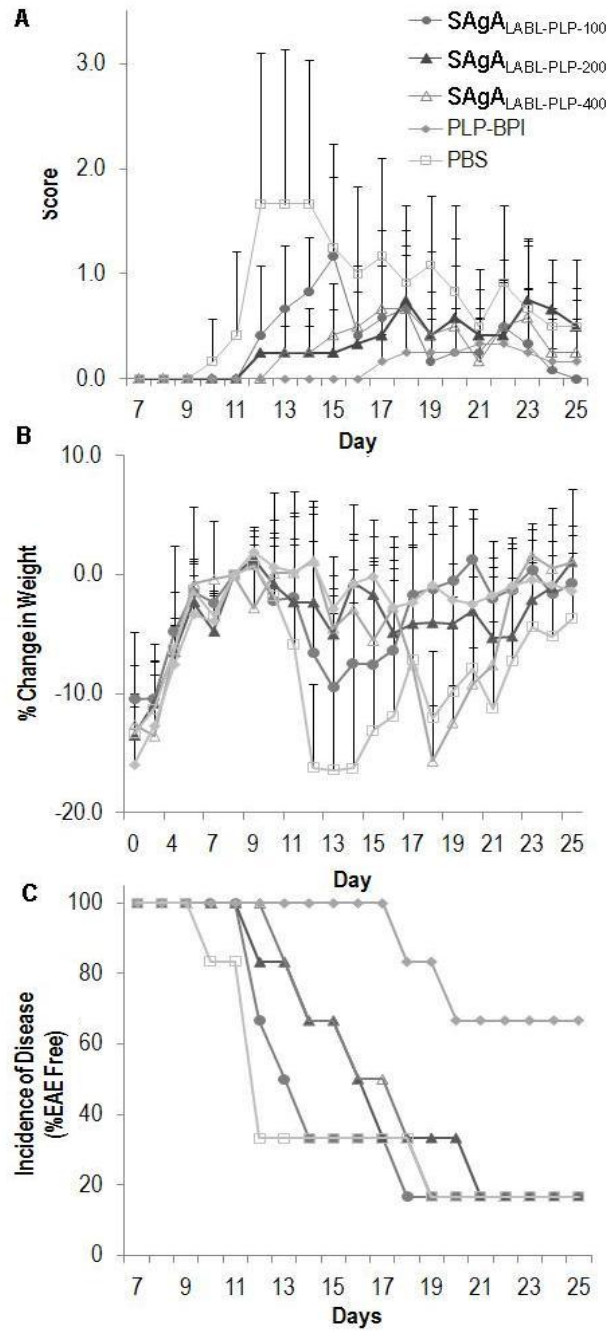


Figure 4: Effect of increasing concentration of PLP (100, 200, and 400 nMol) delivered on SAg_{LABL-PLP}. The data show that 200 nMol and 400 nMol PLP dose (SAg_{LABL-PLP-200}) performed best in (A) clinical disease score, (B) % change in body weight, and (C) incidence of disease. Differences that were statistically significant are summarized in Table 4.

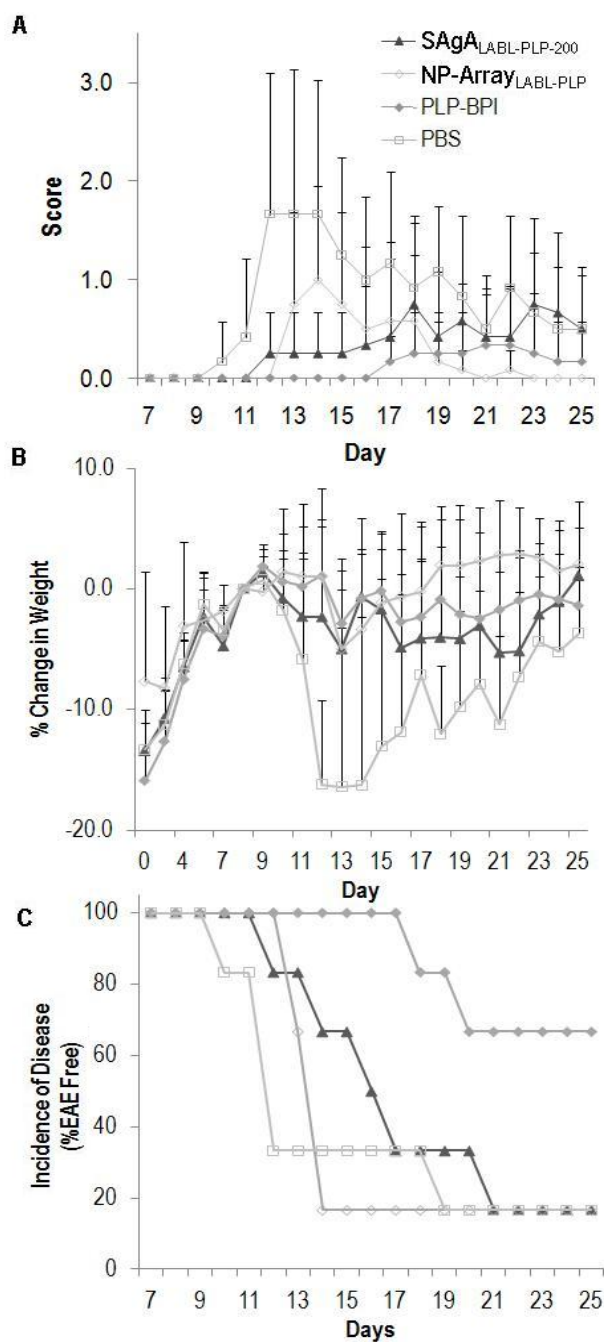


Figure 5: Effect of HA or NP scaffold on clinical efficacy. The data show that the HA array (SAgA_{LABL-PLP-200}) performed better than NP based array (NP-Array_{LABL-PLP}) in (A) clinical disease score, (B) % change in body weight, and (C) incidence of disease. Differences that were statistically significant are summarized in Table 4.

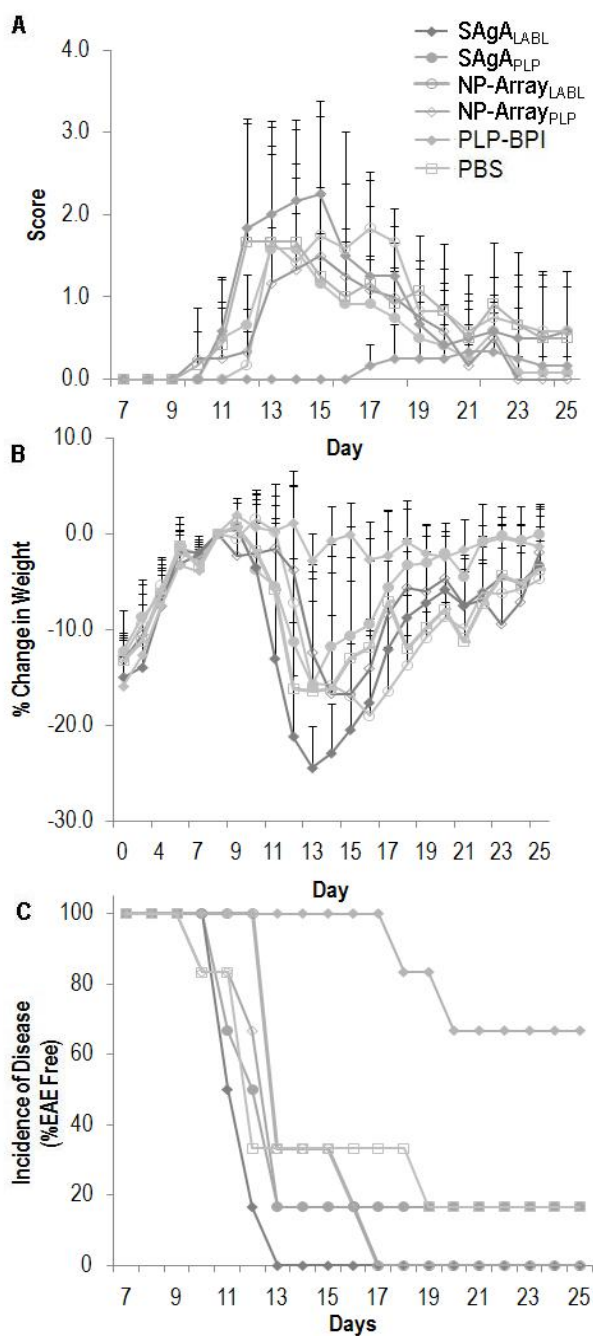


Figure 6: Effect of multivalent delivery of only antigen (PLP) or only cell-adhesion inhibitor ligand (LABL) on HA or NP scaffolds. Neither the multivalent antigen nor the multivalent cell-adhesion inhibitor therapies provided significant suppression of disease as illustrated by overlapping (A) clinical disease score, (B) % change in body weight, and (C) incidence of disease results. Differences that were statistically significant are summarized in Table 4.

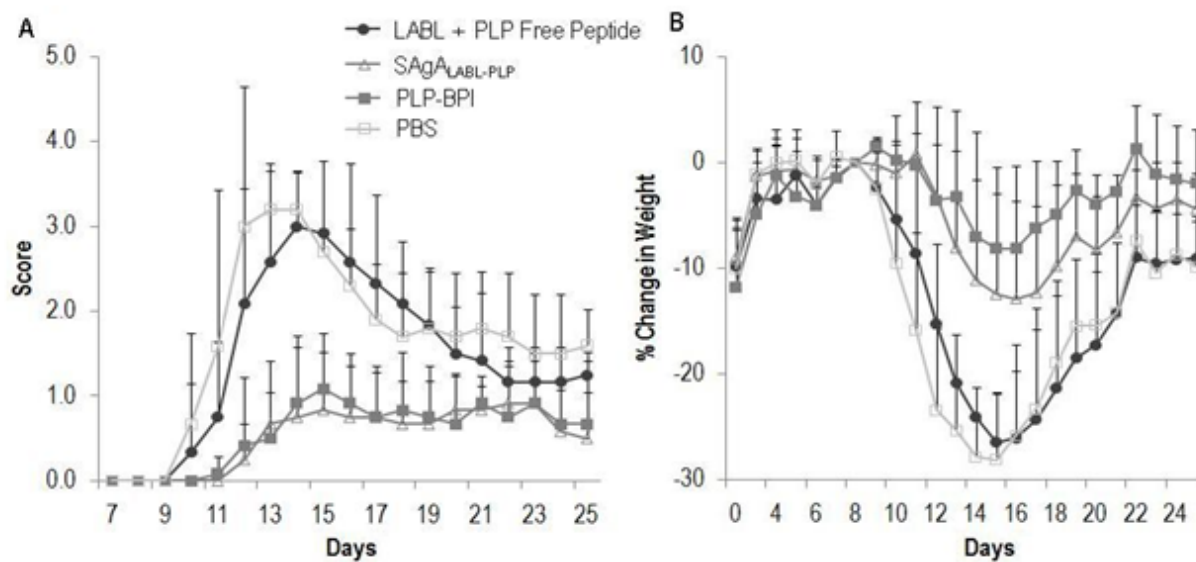
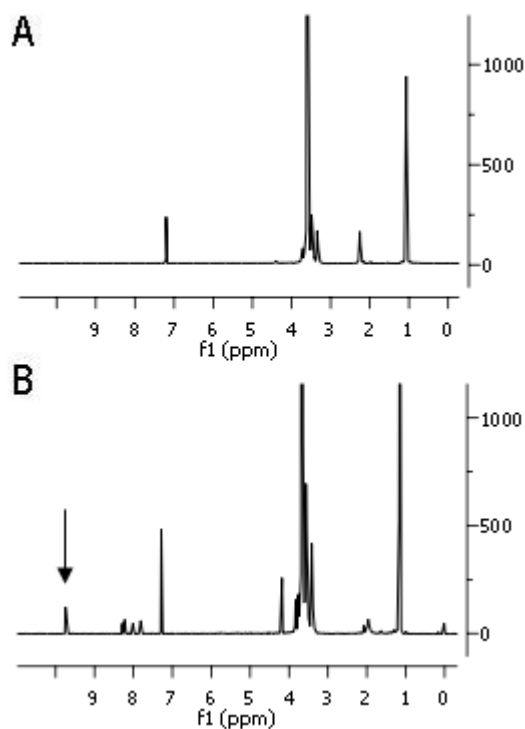


Figure 7: Effect of mixture of free LABL and PLP peptide. Mixture of free peptides provided no suppression of disease as illustrated by overlapping (A) clinical disease score, (B) % change in body weight with the negative PBS control.

Supplementary Figures

Supplementary Figure I: ^1H NMR spectra for Pluronic[®] (A) F108-OH and (B) F108-CHO showing conversion of $-\text{OH}$ end groups to CHO .

Chapter 4

Optimization of SAgAs – Effect of target and size

INTRODUCTION

Investigation into the root cause(s) of multiple sclerosis requires an understanding of the role that CD4⁺/CD8⁺ T cells, B cells, and monocytes play in disease progression. These immune cell populations participate in antigen recognition and processing, immune cell proliferation, antibody production, and trafficking into the central nervous system (CNS), resulting in disease exacerbation. (1-3) Acknowledging this, therapeutics have aimed to disrupt antigen recognition and cell proliferation pathways, or to prevent transport of leukocytes into the CNS to avoid further damage. The multiple sclerosis (MS) therapy Copaxone® utilizes a polymeric antigen which appears to induce the proliferation of regulatory T cells (T_{regs}). (4-6) Alternatively, a monoclonal antibody therapy, TYSABRI®, demonstrates that blocking integrin $\alpha 4 \beta 1$ prevented extravasation of CD8⁺ T cells into the CNS and slowed disease progression in patients with MS. (7-10) While these therapies provide relief from the symptoms of MS, the risk of multiple serious side effects such as severe immune suppression (11) and life-threatening secondary infections (12) still exists. Because of these shortcomings, alternative treatment pathways are being investigated. As a new strategy, Soluble Antigen Arrays (SAGAs) aim to interrupt cell signaling during antigen recognition that leads to immune cell proliferation and antibody production.

Antigen-specific treatments, (13) much like vaccines, look to utilize antigen to induce specific immune responses. Presentation of disease-specific antigen as repeating patterns, either in high local concentrations or in frequent low doses can induce an inflammatory immune response or tolerance. (14-17) Many studies have focused on the physical context of antigen presentation and the effect on the immune response. (18-19) Recent research has aimed to induce, modify, or disrupt the formation of the immunological synapse often by manipulating the physical or chemical properties of the antigen. (20-24) One example, a “bi-functional peptide inhibitor” (PLP-BPI), was synthesized by fusing an MS antigen derived from proteolipid protein, PLP, and a peptide (LABL) that binds intracellular adhesion molecule-1 (ICAM-1). PLP-BPI

suppressed Experimental Autoimmune Encephalomyelitis (EAE) significantly compared to controls. When the ICAM-1 targeting peptide was replaced by a peptide (IBR) that binds the ICAM-1 receptor leukocyte-associated function antigen-1 (LFA-1), preliminary data suggested an increase in efficacy, however, this is still being investigated. (25-26)

SAGAs aim to tailor both the physical and chemical context of antigen presentation. Initial SAGA design utilized LABL to target ICAM-1 and a therapeutic size of ~80 kDa in order to encourage multivalent interaction with immune cells while avoiding rapid clearance after subcutaneous (SC) injection. (27) Therefore, SAGAs targeting either ICAM-1 or LFA-1 were explored here. Controlling SAGA location was also expected to be important in treating MS since antigen recognition has been shown to occur in the draining lymphatics for the CNS. (28) The lymphatics present a unique, highly organized microenvironment rich in subpopulations of APCs, T cells, and B cells participating in disease progression. (29) SAGA size was expected to affect the drainage into, residence time within, and clearance from lymph nodes, thereby potentially altering the clinical immune response. Thus, the chemical (targeting) and physical (size) characteristics of SAGAs were explored as a means to suppress EAE.

In EAE, disease progression is characterized by suspected protein antigens, such as proteolipid protein (PLP), myelin basic protein (MBP), and myelin oligodendrocyte glycoprotein (MOG), (30) acting as immunogenic epitopes and activating naïve CD4⁺ T-cells. After antigen presentation by pAPCs, these activated CD4⁺ T cells can differentiate into Th1 or Th17 effector cells. More importantly, these events lead to the production of specific cytokines such as IL-2, IFN- γ , and TNF- α . In addition, Th17 cells secrete cytokines such as IL-17, and are further activated by cytokines IL-6, IL-23, and TGF- β . (1, 31) Disease suppression is expected to be related to the proliferation of adaptive regulatory T cells (T_{regs}) which may be linked to the expression of immunosuppressive cytokines, IL-10 and/or TGF- β . (32-33) Here, IL-2, IL-4, IL-10, IL-17, IFN- γ , and TNF- α concentrations in blood were monitored to help define the immune response to SAGAs differing in size or target (ICAM-1 or LFA-1). (34)

MATERIALS AND METHODS

Materials. Hyaluronic acid (HA), with an average molecular weight of 17 and 31 kDa were purchased from Lifecore. Analytical grade acetonitrile, synthesis grade trifluoro acetic acid (TFA), and PBS buffer were purchased from Fisher Scientific. Research grade sodium acetate, acetic acid, and D₂O and heparin were purchased from Sigma. Water was provided by a Labconco Water PRO PS ultrapure water purification unit.

Mice. Four – 6 weeks old SJL/J (H-2s) female mice were purchased from The Jackson Laboratory. Animals were housed under specified pathogen-free conditions at The University of Kansas Animal Care Facility. The University of Kansas Institutional Animal Care and Use Committee approved all protocols involving live mice.

Peptide Synthesis. 9-fluorenylmethyloxycarbonyl-protected amino acid chemistry on polyethylene glycol-polystyrene resins was used to synthesize the *aminoxy* peptides. Peptides synthesized for this study were aminoxy-LABL (aminoxy-ITDGEATDSG, *Ao-LABL*), a ligand of ICAM-1, aminoxy-IBR (aminoxy-GGGPRGGVS, *Ao-IBR*), a ligand of LFA-1, and aminoxy-PLP (aminoxy-HSLGKWLGHDPKF, *Ao-PLP*), an antigen derived from proteolipid protein amino acids 139-151 (PLP₁₃₇₋₁₅₁). Each peptide was deprotected, cleaved from resin, and isolated by precipitation in ether. Preparatory High Performance Liquid Chromatography (HPLC) was employed to purify the peptides, followed by lyophilization. Purity/content and peptide identity were verified using analytical HPLC and Mass Spectroscopy. PLP-BPI, a fusion of PLP and LABL (HSLGKWLGHDPKF-AcGAcGAc-ITDGEATDSG), was synthesized and purified as previously reported.⁽³⁵⁾

Reaction of Aminoxy Peptides to Polymers. The HA scaffolds were dissolved into 20 mM Acetate buffer (pH 5.5 ± 0.1 pH units) and aminoxy reactive peptide(s) added. When multiple peptide species were used, each was weighed separately, and then both peptides were added simultaneously. Reaction solution pH was adjusted back to pH 5.5 ± 0.1 pH units after addition

of the peptide(s). Reaction solutions were stirred at for ~ 16 hr. After the reaction, the soluble antigen array (SAgA) product was purified by extensive dialysis to remove any unreacted peptide, and then lyophilized.

High Performance Liquid Chromatography. Reversed phase HPLC (SHIMADZU) using a Vydac HPLC protein and peptide C18 column was used to quantified conjugated peptide. The HPLC system was made up of an SCL-20A SHIMADZU system controller, LC-10AT VP SHIMADZU liquid chromatograph, SIL-10A XL SHIMADZU auto-injector set at 75 μ L injection volume, DGU-14A SHIMADZU degasser, sample cooler, and SPD-10A SHIMADZU UV-vis detector (220 nm). The HPLC-UV system was controlled by a personal computer equipped with SHIMADZU class VP software. A gradient elution was conducted at constant flow of 1 mL/min, from 100% A to 35% A (corresponding to 0% B to 65% B) over 50 min, followed by an isocratic elution at 75% B for 3 min. The mobile phases were (A) acetonitrile-water (5:95) with 0.1% TFA and (B) acetonitrile-water (90:10, v/v) with 0.1% TFA. After each analysis, the cartridge was equilibrated at initial conditions at 1 mL/min flow rate for 5 min with A.

Preparation of Near Infrared Dye IR-820. To prepare the dye, 125 mg 6-aminocaproic acid was dissolved in dry DMF (20mL). TEA (130 μ L) was added and the mixture was allowed to stir under argon for ~5 min. Then, 500 mg IR-820 was added. A reflux condenser was attached and the mixture was heated to 85°C for 3 hr in the dark. After the reaction the solvent was removed using a rotovap (Bruker) and placed under vacuum over night to dry.

Conjugation of IR-820 to Hyaluronic Acid. IR-820-5aminohexanoic acid dye was dissolved into water. EDC was added and the solution pH was adjusted to 4.5. Then, DMAP was added and the solution was stirred, in the dark, for 5 min. After activation of IR-820 (5 min), hyaluronic acid was added to the flask and the solution was stirred in the dark, for 48 hours. The product was purified by dialyzing against 95% EtOH for 8 hours, then against water twice (8 Hours a time) in the dark. The retentate was lyophilized and the dye content of the product was confirmed using NMR (Supplementary Table 1).

Nuclear Magnetic Resonance Spectroscopy. For dye content analysis, samples were dissolved in D₂O to a concentration of 10 mg/mL. H1 spectra were acquired on a Bruker 400MHz spectrometer at 25 °C.

Induction of EAE and Therapeutic Study. Four – 6 week-old SJL/J female mice were immunized subcutaneously (s.c) with 200 µg of PLP_{139–151} in a 0.2 mL emulsion composed of equal volumes of complete Freund's adjuvant (CFA) containing killed *Mycobacterium tuberculosis* strain H37RA (final concentration of 4 mg/mL; Difco) and phosphate-buffered saline (PBS) containing PLP. The PLP_{139–151}/CFA emulsion was administered to regions above the shoulders and the flanks (total of four sites; 50 µL at each injection site). Additionally, 200 ng/100 µL of pertussis toxin (List Biological Laboratories Inc.) was injected intraperitoneally (i.p.) on the day of immunization (day 0) and 2 days post-immunization. Mice received s.c. injections of each sample, equivalent to 200 nMol PLP /100 µL, on days 4, 7, 10. One hundred µL of each vehicle was injected for all samples and controls. Disease progression was evaluated blindly by the same observer using clinical scoring as follows: 0, no clinical signs of the disease; 1, tail weakness or limp tail; 2, paraparesis (weakness or incomplete paralysis of one or two hind limbs); 3, paraplegia (complete paralysis of two hind limbs); 4, paraplegia with forelimb weakness or paralysis; and 5, moribund (mice were euthanized if they were found to be moribund). Body weight was also measured daily.

Cytokine Analysis. Blood samples were taken from each mouse via mandibular bleeds (~100 uL) on days 0, 6, 12, 18, 25. To ensure there was enough sample to perform ELISA cytokine testing blood from, two mice within the same group was pooled at each time point for a total of four samples per group. Samples were collected in heparin-containing tubes and centrifuged to separate red blood cells. Plasma was collected and sent for cytokine analysis to the Cytokine Core Laboratory at the University of Maryland. The cytokines analyzed were IL-2, IL-4, IL-10, IL-17, TNF-α, and TGF-β.

***In vivo* Imaging.** *In vivo* imaging was completed using the Maestro Imaging Suite. Animals were anesthetized using an isoflurane vaporizer and IR-820 labeled SAgA was injected s.c. at the base of the neck. After injection images were taken of the animal's top, left, bottom, and right side by rotating the animal in the exposure pane. The animal was imaged at defined time points over a 24 hour period to track the drainage and clearance of the SAgA from the injection site.

Statistical Analysis. Statistical differences were determined by comparing treated groups to the negative control (PBS) for clinical disease score and body weight. A one-way analysis of variance (ANOVA) followed by Fisher's least significant difference was applied to these data. For individual clinical scores and cytokine values T test was employed. All analyses were performed using GraphPad Software (GraphPad Software Inc.).

RESULTS

Characterization of Polymeric Soluble Antigen Arrays. The concentration of peptide grafted to the HA backbone was quantified by HPLC. Peptide was released from HA by incubating the SAgA product in pH 2 mobile phase buffer at room temperature. Chromatographs demonstrated the presence of the *Ao-LABL* or *Ao-IBR* peptide, and the *Ao-PLP* peptide at approximately the desired 1:1 ratio for all products. All peptides were conjugated at a high level of efficiency, >90% (Table 1).

The therapeutic efficacy of various SAgAs was evaluated in the EAE model induced in SJL/J mice. The study design is outlined in Table 2. Typically, disease onset occurs at approximately day 8 and progresses to remission around day 20. Disease is manifested by physical signs, such as weakness, paralysis of the tail and limbs, and loss of body weight. Injections of each sample were given subcutaneously at the base of the neck, on days 4, 7, 10.

Effect of Cell-adhesion Target on Suppression. SAgAs targeting either ICAM-1 (SAgA_{LABL-PLP}) or LFA-1 (SAgA_{IBR-PLP}) performed significantly better than the negative PBS control in

clinical score ($p < 0.01$, for days 14 & 17-19 for both) (Figure 1-A). Additionally, the mice treated with the targeted SAgAs also had significantly better maintenance of body weight ($p < 0.05$, for days 15-21 for SAgA_{LABL-PLP} and day 18 for SAgA_{IBR-PLP}) compared to the negative control PBS group (Figure 1-B). Of all the treated groups, only the SAgA_{IBR-PLP} had mice that never developed EAE as identified by a clinical score of ≥ 1 (Figure 1-C). This data compared well to the positive PLP-BPI control and no statistical difference was seen between treatments with SAgAs compared to the positive control.

Effect of SAgA Size on Suppression. Both the 50 kDa and 80 kDa SAgA_{LABL-PLP} and the 50 kDa and 80 kDa SAgA_{IBR-PLP} inhibited the progression of EAE as evidenced by very low clinical scores compared to the negative PBS control (Figure 2-A). Clinical suppression was significantly improved over PBS treatment for the 50 kDa and 80 kDa SAgA_{LABL-PLP} ($p < 0.05$, for days 14 & 17 and 14 & 17-19, respectively) as well as the 50 kDa and 80 kDa SAgA_{IBR-PLP} ($p < 0.05$, for days 14 & 17-19 for both). The treated mice also had better maintenance of body weight (Figure 2-B) compared to the negative control PBS group for all tested groups. Complete statistics are outlined in Table 2. Additionally, the smaller 50 kDa SAgA_{IBR-PLP} delayed the onset of disease better than the 80 kDa SAgA_{IBR-PLP} ($p < 0.05$, day 11) with initiation of disease occurring two days later with the 50 kDa SAgA_{IBR-PLP}. A high percentage of animals treated with the 50 kDa SAgA_{IBR-PLP} never developed clinical scores ≥ 1 (Figure 2-C). This data compared well to the positive PLP-BPI control and no statistical difference was seen between treatments with SAgAs as compared to the positive control.

In vivo imaging of SAgAs. Both the 50 and 80 kDa SAgA_{LABL-PLP} were imaged and compared to a 30 kDa HA (the 80 kDa backbone) and a 70 kDa HA that was similar in Mw to the final products. After injection of the IR820-labeled HA or SAgA_{LABL-PLP}, the drainage from the injection site was tracked and images were acquired over 24 hours (Figure 3). The 30 kDa HA (Figure 4-A) appeared to drain from the injection site and into the local lymph nodes quickly, and was cleared by 1440 min. The 70 kDa HA (Figure-4B) showed a relatively shorter drainage

time with the labeled HA detectable only until 500 min. For the labeled SAgA conjugates, the drainage time more closely resembled the slow drainage of the smaller 30 kDa HA rather than the 70 kDa HA. The 50 kDa SAgA_{LABL-PLP} showed drainage away from the injection site and suggested drainage into the local lymphatics. Clearance was not achieved until 1440 min, similar to the 30 kDa HA. The larger 80 kDa SAgA_{LABL-PLP} showed similar drainage into the lymphatics, but it was still visible even after 1260 minutes. While these results are qualitative, they do provide some insight into the location of the SAgA conjugates at different time points.

Effect of SAgA on Cytokine Profile. The plasma samples were analyzed for 6 cytokines; IL-2, IL-4, IL-10, IL-17, TNF- α , and IFN- γ . Baseline levels of each cytokine were measured at Day 0 before disease induction. Within each testing group, blood was pooled from two mice resulting in an n=4. When statistics were performed deviations from n=4 due to samples being below the level of detection for cytokine measurements are noted. IL-2 and IL-10 were below the limit of detection in all samples.

Examination of IL-4, IL-17, TNF- α , and IFN- γ suggested that treatment with SAgAs led to differences in the cytokine production profiles when compared to both the PBS and PLP-BPI controls. The largest differences were seen with the levels of IFN- γ , TNF- α , and IL-17 data, while smaller differences were seen with IL-4 levels (Figure 4). Mice receiving PBS had very high average concentrations of IFN- γ by day 6 (72 pg/mL); however, groups treated with SAgAs of PLP-BPI suppressed IFN- γ production. The PLP-BPI (31 pg/mL) and the 50 kDa SAgA_{IBR-PLP} (38 pg/mL) treatments provided moderate suppression with an average of ~40% reduction in peak expression of IFN- γ on Day 6. The lowest IFN- γ levels were seen with both the 50 and 80 kDa SAgA_{LABL-PLP} (12 and 14 pg/mL respectively) and the 80 kD SAgA_{IBR-PLP} (6 pg/mL), correlating to an ~80-90% reduction compared to the PBS controls. When a T-test was performed for Day 6 measurements, the 50 and 80 kDa SAgA_{LABL-PLP} and 80 kDa SAgA_{IBR-PLP} were significantly different than the PBS. For the 80 kDa SAgA_{LABL-PLP} and PBS groups n=3.

For both TNF- α and IL-17, treatment with SAgA or PLP-BPI led to an increase in the circulating cytokine concentrations compared to the PBS control. Similar to the IFN- γ data, peak concentrations of TNF- α occurred on day 6 for the PBS samples; however, these levels were very low at 1.8 pg/mL. The PLP-BPI reached 3.1 pg/mL of TNF- α on day 6. The 50 kDa SAgA_{LABL-PLP} (3.7 pg/mL), 80 kDa SAgA_{LABL-PLP} (3.4 pg/mL), and 80 kDa SAgA_{IBR-PLP} (2.6 pg/mL) also reached peak levels on day 6. The 50 kDa SAgA_{IBR-PLP} showed peak concentrations at days 6 and 18 (3.7 & 4.2 pg/mL).

The IL-17 data for the PBS control showed a peak concentration at day 6 (23 pg/mL). The 80 kDa SAgA_{IBR-PLP} (45 pg/mL) and the PLP-BPI (40 pg/mL) control gave slightly elevated levels of IL-17; however, the PLP-BPI maintained elevated levels through day 12 (31 pg/mL), then returned toward baseline. Interestingly, peak concentrations at both days 6 and 18 were seen for the 50 kDa SAgA_{IBR-PLP} (45 & 82 pg/mL), and both the 50 kDa SAgA_{LABL-PLP} (66 & 21 pg/mL) and 80 kDa SAgA_{LABL-PLP} (45 & 41 pg/mL).

Finally, IL-4 concentrations, though low, showed similar results for all samples (0.25-0.35 pg/mL), except for the 50 kDa SAgA_{LABL-PLP} and 80 kDa SAgA_{IBR-PLP}, which had increased levels. The IL-4 levels for 50 kDa SAgA_{LABL-PLP} were similar to all other samples on day 6 (0.25 pg/mL), but, increased on day 12 (1.1 pg/mL). The 80 kDa SAgA_{IBR-PLP} level decreased on day 6 to a concentration of 0.73 pg/mL. After day 6, the 80 kDa SAgA_{IBR-PLP} IL-4 level continued to decrease, however, became elevated at the study end (0.2 pg/mL).

DISCUSSION

Antigen recognition and the response propagated by immune cells are key events in progression of autoimmune diseases such as multiple sclerosis. Many of the current therapeutic approaches attempt to interfere with these events either directly or through the manipulation of secondary pathways such as cytokine production. Traditionally, these therapeutic pathways have been targeted independently; for example, monoclonal Abs targeting

specific receptors (e.g. cell-adhesion or co-stimulation) or altered peptide ligands interfering with antigen presentation. Unfortunately, these treatments often lack long term efficacy or result in deleterious side effects, requiring a new therapeutic strategy.

SAGAs were rationally designed to display multiple copies of antigen alongside inhibitors of immune cell adhesion. A “bi-functional peptide inhibitor” developed by Siahaan and others, used a fusion peptide of the EAE disease-specific antigen (PLP) and a cell-adhesion inhibitor (LABL) connected via a linker. The goal of this construct was interference with the formation of the immunological synapse. Reports showed that PLP-BPI molecules achieved clinical efficacy in EAE by preventing APC activation of naïve T cells.(1, 25, 35-36) Here, this validated molecular strategy was paired with multivalent antigen display. Seminal papers from Dintzis and others systematically demonstrated that immunosuppression could be achieved by controlling the number and density of grafted antigens along the polymer. (37-39) The “soluble antigen arrays” investigated in this research aimed to combine the success of both the PLP-BPI and multivalent antigen arrays by presenting multiple copies of both antigen and cell-adhesion inhibitors.

Previously, SAGAs that presented both the EAE antigen, PLP, and the ICAM-1-targeting peptide, LABL, delayed the onset of disease and lowered EAE clinical scores, similar to that of PLP-BPI (Chapter 3). Unpublished results from additional studies suggested that PLP-BPIs that targeted LFA-1 (40-41) rather than ICAM-1 were able to suppress EAE with greater efficacy. Therefore, the effect of substituting IBR for LABL on SAGAs was hypothesized to further improve efficacy. When IBR was substituted for LABL on the SAGAs, however, no significant change in efficacy was seen. This result, while not in agreement with what had been observed with PLP-BPI, was not unexpected. In previous work, dendritic cells (DCs) treated with nanoparticles displaying LABL or IBR showed a similar reduction in T cell binding, perhaps suggesting minimal differences between these two cell-adhesion inhibitors when presented as multivalent arrays. (42) Here, clinical efficacy was similar whether the SAGAs displayed the cell-

adhesion inhibitor LABL or IBR. This observation led to the investigation of alternative SAgA characteristics that could improve therapeutic performance.

Next, SAgA Mw was reduced in an effort to promote drainage to regional lymph nodes and animal response was monitored for SAgAs targeting either ICAM-1 or LFA-1. The efficacies of all the different SAgAs were similar to one another as well as to the PLP-BPI positive control. While the clinical scores were similar, the smaller SAgAs delayed the onset of disease and decreased the incidence of disease. Smaller arrays with ~20 total grafted peptides provided increased efficacy over larger arrays with ~32 grafted peptides. While the molecular architecture is no doubt important, the improvement from a small change in Mw motivated further investigation into the post-injection fate of the SAgA materials (Figure 3). Real-time, *in vivo* imaging results showed that differences in SAgA Mw indeed affected the relative rate of drainage from the injection site to the regional lymphatics. Smaller 50 kDa SAgAs could no longer be detected while 80 kDa SAgAs remained visible after 24 hours in what appeared to be the local lymphatics near the injection site. Thus, more rapid drainage away from the injection site and toward the lymphatics may explain the difference clinical results.

To define the immunological mechanisms behind the observed responses, plasma samples were taken from each mouse and six different cytokines were monitored throughout the course of the *in vivo* studies. Cytokines provide insight into cellular responses and possible mechanistic pathways. IL-2 and IL-10 were below the limit of detection; however, this was not unexpected as circulating levels of these cytokines are recognized to be very low. Compared to PBS, all treatments affected the IL-4, IL-17, TNF- α , and IFN- γ levels during the course of the study. Control mice treated with PBS produced high levels of IFN- γ , while the levels in mice treated with SAgAs or PLP-BPI were suppressed. High levels of IFN- γ are associated with a Th1 phenotype, which dampens the Th2 response. (43) In the presence of the SAgAs, the phenotype seemed to be skewed away from an IFN- γ promoted Th1 phenotype and towards a

Th2 response. Of equal importance, levels of TNF- α were increased in the treated groups. Since TNF- α can induce apoptosis in the CD4⁺ T cell population, future studies will aim to determine apoptosis in T cells of the treated animals. (44) Levels of IL-4 did not vary significantly between the treated groups and the PBS controls. With the exception of the group treated with 50 kDa SAgA_{LABL-PLP}, IL-4 may therefore not contribute significantly to the observed differences between the groups.

Cytokines IL-17, TNF- α , and IFN- γ are typically seen as pro inflammatory in autoimmune diseases while IL-4 is expected to dampen the Th2 response, stimulating immune suppression or tolerance. Recent studies, however, have suggested that cytokines such as IL-17 and TNF- α can induce both inflammatory and/or anti-inflammatory or tolerogenic responses depending on the other cytokines expressed. (32, 45) These recent studies go against conventional thinking that IL-17, a direct measurement of Th17 population, is a measurement of disease progression. Although the negative PBS control had high levels of serum IFN- γ concentration, the same group produced low levels of both TNF- α and IL-17, cytokines traditionally viewed as pro inflammatory. In contrast, the observed reduction in IFN- γ in the treated groups was associated with a corresponding increase in IL-17 and alteration in TNF- α . Historically, Th17 and Th1/Th2 responses have been observed as independent pathways, however, recent research suggests Th17 cell populations can exhibit plasticity and produce IL-17 or IFN- γ . In the case of Th17-mediated autoimmune diseases such as MS this plasticity could lead to a tolerogenic response, (32) a hypothesis that would fit the observed data well. It is worth noting that IL-10 signaling in regulatory T cells mediates suppression of the Th17 phenotype during inflammation. (46-47) This is accomplished by up regulation of the IL-10 receptor on the Th17 cells during an immune response. As mentioned, IL-10 was undetectable in any group of mice, therefore, it is currently unclear if IL-10 levels can be regulated by SAgAs.

The bimodal cytokine distributions for certain SAgA therapeutics were perhaps the most intriguing data arising from this study. Multiple SAgA species elicited a bimodal production cycle of TNF- α and IL-17 cytokines. Concentration maximums for these cytokines at days 6 and 18 could suggest initiation of the adaptive or long-term immune response. The samples that showed the largest peaks, 50 kDa SAgA_{IBR-PLP}, 50 kDa SAgA_{LABL-PLP}, and 80 kDa SAgA_{LABL-PLP}, also exhibited very effective disease suppression. While all groups performed similarly with regards to clinical score and body weight maintenance, this variation in the cytokine response may play a vital role in an immune response leading to long-term efficacy.

CONCLUSIONS

SAgAs targeting ICAM-1 or LFA-1 were evaluated and either target provided similar suppression of EAE. Decreasing the Mw of SAgAs from 80 kDa to 50 kDa delayed the disease onset. *In vivo* imaging revealed differences in drainage profiles between the 50 kDa and 80 kDa SAgAs with the larger complex having extended residence near the injection site. Treatment with 50 and 80 kDa SAgA_{LABL-PLP} and 80 kDa SAgA_{IBR-PLP} demonstrated decreased production of the pro inflammatory cytokine IFN- γ compared to the PBS control. Additionally, the 50 kDa SAgAs demonstrated differences in the production of IL-17, while the 50 kDa SAgA_{LABL-PLP} and 80 kDa SAgA_{IBR-PLP} altered the TNF- α profile compared to PBS. The physical characteristics of SAgAs had a significant impact on the chemical outcomes and immune responses observed in the EAE mouse model.

REFERENCES:

1. Manikwar P, Kiptoo P, Badawi AH, Büyüktimkin B, Siahaan TJ. Antigen-specific blocking of CD4-specific immunological synapse formation using BPI and current therapies for autoimmune diseases. *Medicinal Research Reviews*. 2011;n/a-n/a.
2. Wohler JE, Smith SS, Barnum SR. $\gamma\delta$ T cells: The overlooked T-cell subset in demyelinating disease. *Journal of Neuroscience Research*. 2010;88(1):1-6.
3. Wohler JE, Smith SS, Zinn KR, Bullard DC, Barnum SR. $\gamma\delta$ T cells in EAE: Early trafficking events and cytokine requirements. *European Journal of Immunology*. 2009;39(6):1516-26.
4. Aharoni R, Teitelbaum D, Leitner O, Meshorer A, Sela M, Arnon R. Specific Th2 cells accumulate in the central nervous system of mice protected against experimental autoimmune encephalomyelitis by copolymer 1. *Proc Natl Acad Sci U S A*. 2000;97(21):11472-7.
5. Senti G, Prinz Vavricka BM, Erdmann I, Diaz MI, Markus R, McCormack SJ, et al. Intralymphatic allergen administration renders specific immunotherapy faster and safer: a randomized controlled trial. *Proc Natl Acad Sci U S A*. 2008;105(46):17908-12.
6. Steinman L, Conlon P. Antigen specific immunotherapy of multiple sclerosis. *J Clin Immunol*. 2001;21(2):93-8.
7. Moriyama H, Yokono K, Amano K, Nagata M, Hasegawa Y, Okamoto N, et al. Induction of tolerance in murine autoimmune diabetes by transient blockade of leukocyte function-associated antigen-1/intercellular adhesion molecule-1 pathway. *J Immunol*. 1999;157:3737-43.
8. Kavanaugh AF, Davis LS, Jain RI, Nichols LA, Norris SH, Lipsky PE. A phase I/II open label study of the safety and efficacy of an anti-ICAM-1 (intercellular adhesion molecule-1; CD54) monoclonal antibody in early rheumatoid arthritis. *J Rheumatol*. 1996;23(8):1338-44.
9. Schulze-Koops H, Lipsky PE, Kavanaugh AF, Davis LS. Elevated Th1- or Th0-like cytokine mRNA in peripheral circulation of patients with rheumatoid arthritis. Modulation by treatment with anti-ICAM-1 correlates with clinical benefit. *J Immunol*. 1995;155(10):5029-37.
10. Steinman L. Blocking adhesion molecules as therapy for multiple sclerosis: natalizumab. *Nat Rev Drug Discov*. 2005;4(6):510-8.
11. Sheridan C. Tysabri raises alarm bells on drug class. *Nat Biotechnol*. 2005;23(4):397-8.
12. Langer-Gould A, Steinman L. Progressive multifocal leukoencephalopathy and multiple sclerosis: lessons from natalizumab. *Curr Neurol Neurosci Rep*. 2006;6(3):253-8.
13. Dolgin E. The inverse of immunity. *Nat Med*. 2010;16(7):740-3.
14. Kool M, Petrilli V, De Smedt T, Rolaz A, Hammad H, van Nimwegen M, et al. Cutting edge: alum adjuvant stimulates inflammatory dendritic cells through activation of the NALP3 inflammasome. *J Immunol*. 2008;181(6):3755-9.
15. Ahmed N, Gottschalk S. How to design effective vaccines: lessons from an old success story. *Expert Rev Vaccines*. 2009;8(5):543-6.
16. Rolland JM, Gardner LM, O'Hehir RE. Allergen-related approaches to immunotherapy. *Pharmacol Ther*. 2009;121(3):273-84.
17. Lisak RP, Zweiman B, Blanchard N, Rorke LB. Effect of treatment with Copolymer 1 (Cop-1) on the in vivo and in vitro manifestations of experimental allergic encephalomyelitis (EAE). *J Neurol Sci*. 1983;62(1-3):281-93.
18. Dustin ML. The cellular context of T cell signaling. *Immunity*. 2009;30(4):482-92.
19. Sant AJ, Chaves FA, Jenks SA, Richards KA, Menges P, Weaver JM, et al. The relationship between immunodominance, DM editing, and the kinetic stability of MHC class II:peptide complexes. *Immunol Rev*. 2005;207:261-78.
20. Mossman KD, Campi G, Groves JT, Dustin ML. Altered TCR signaling from geometrically repatterned immunological synapses. *Science*. 2005;310(5751):1191-3.
21. Hartman NC, Nye JA, Groves JT. Cluster size regulates protein sorting in the immunological synapse. *Proc Natl Acad Sci U S A*. 2009;106(31):12729-34.

22. Dustin ML. The immunological synapse. *Arthritis Res.* 2002;4(Suppl 3):S119–25.
23. Dustin ML, Shaw AS. Costimulation: Building an immunological synapse. *Science.* 1999;283(5402):649–50.
24. Bromley SK, Iaboni A, Davis SJ, Whitty A, Green JM, Shaw AS, et al. The immunological synapse and CD28-CD80 interactions. *Nat Immunol.* 2001;2(12):1159–66.
25. Manikwar P TB, Shinogle H, Moore DS, Zimmerman T, Blanco F, Siahaan TJ. Utilization of I-domain of LFA-1 to Target Drug and Marker Molecules to Leukocytes. *Theranostics.* 2011;1:277-89.
26. Yusuf-Makagiansar H, Makagiansar IT, Hu Y, Siahaan TJ. Synergistic inhibitory activity of [alpha]- and [beta]-LFA-1 peptides on LFA-1/ICAM-1 interaction. *Peptides.* 2001;22(12):1955-62.
27. Swartz MA, Hubbell JA, Reddy ST. Lymphatic drainage function and its immunological implications: From dendritic cell homing to vaccine design. *Seminars in Immunology.* 2008;20(2):147-56.
28. Aloisi F, Ria F, Adorini L. Regulation of T-cell responses by CNS antigen-presenting cells: different roles for microglia and astrocytes. *Immunology Today.* 2000;21(3):141-7.
29. Junt T, Scandella E, Ludewig B. Form follows function: lymphoid tissue microarchitecture in antimicrobial immune defence. *Nat Rev Immunol.* 2008;8(10):764-75.
30. S. S. Candidate autoantigens in multiple sclerosis. *Mult Scler.* 1999;5(3):147-60.
31. Mosmann TR CH, Bond MW, Giedlin MA, Coffman RL. Two types of murine helper T cell clone. I. Definition according to profiles of lymphokine activities and secreted proteins. 1986. *J Immunol.* 2005;175(1):5-14.
32. Aranami T YT. Th17 Cells and autoimmune encephalomyelitis (EAE/MS). *Allergol Int.* 2008;57(2):115-20.
33. Nathalie Cools PP, Viggo F. I. Van Tendeloo, and Zwi N. Berneman. Regulatory T Cells and Human Disease. *Clinical and Developmental Immunology.* 2007;2007.
34. Van der Zee JS AR. The role of IgG in immediate-type hypersensitivity. *Eur Respir J Suppl.* 1991;13:91s-6s.
35. Naoki Kobayashi PK, Hitomi Kobayashi, Rahmawati Ridwan, Stefan Brocke, and Teruna J. Siahaan. Prophylactic and Therapeutic Suppression of Experimental Autoimmune Encephalomyelitis by a Novel Bifunctional Peptide Inhibitor. *Clinical Immunology.* 2008;129(1):69-79.
36. Ridwan R, Kiptoo P, Kobayashi N, Weir S, Hughes M, Williams T, et al. Antigen-specific Suppression of Experimental Autoimmune Encephalomyelitis by a Novel Bifunctional Peptide Inhibitor: Structure Optimization and Pharmacokinetics. *J Pharmacol Exp Ther.* 2009.
37. Dintzis HM DR. Profound specific suppression by antigen of persistent IgM, IgG, and IgE antibody production. *Proc Natl Acad Sci U S A.* 1992;89(3):1113-7.
38. Reim JW SD, Watson DC, Dintzis RZ, Dintzis HM. Low molecular weight antigen arrays delete high affinity memory B cells without affecting specific T-cell help. *Mol Immunol* 1996;33(17-18):1377-88.
39. Symer DE DR, Diamond DJ, Dintzis HM. Inhibition or activation of human T cell receptor transfectants is controlled by defined, soluble antigen arrays. *J Exp Med.* 1992;176(5):1421-30.
40. Tejo BA, Siahaan TJ. Solution structure of a novel T-cell adhesion inhibitor derived from the fragment of ICAM-1 receptor: Cyclo(1,8)-Cys-Pro-Arg-Gly-Gly-Ser-Val-Cys. *Biopolymers.* 2009;91(8):633-41.
41. Tejo BA, Tambunan USF, Verkhivker G, Siahaan TJ. Structural Modifications of ICAM-1 Cyclic Peptides to Improve the Activity to Inhibit Heterotypic Adhesion of T cells. *Chemical Biology & Drug Design.* 2008;72(1):27-33.
42. Chittasupho C, Shannon L, Siahaan TJ, Vines CM, Berkland C. Nanoparticles Targeting Dendritic Cell Surface Molecules Effectively Block T Cell Conjugation and Shift Response. *ACS Nano.* 2011;5(3):1693-702.

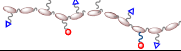
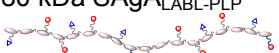
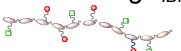
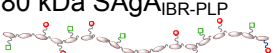
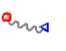
43. Pernis A, Gupta S, Gollob KJ, Garfein E, Coffman RL, Schindler C, et al. Lack of interferon gamma receptor beta chain and the prevention of interferon gamma signaling in TH1 cells. *Science*. 1995;269(5221):245-7.
44. Klein JR. T cell development within the intestinal mucosa: Clues to a novel immune-endocrine network? *Advances in Neuroimmunology*. 1996;6(4):397-405.
45. Leavy O. T cells: Plastic TH17 cells. *Nat Rev Immunol*. 2011;11(3):160-1.
46. Chaudhry A, Samstein Robert M, Treuting P, Liang Y, Pils Marina C, Heinrich J-M, et al. Interleukin-10 Signaling in Regulatory T Cells Is Required for Suppression of Th17 Cell-Mediated Inflammation. *Immunity*. 2011;34(4):566-78.
47. Huber S, Gagliani N, Esplugues E, O'Connor W, Huber Francis J, Chaudhry A, et al. Th17 Cells Express Interleukin-10 Receptor and Are Controlled by Foxp3⁺ and Foxp3⁺ Regulatory CD4⁺ T Cells in an Interleukin-10-Dependent Manner. *Immunity*. 2011;34(4):554-65.

TABLES

Table 1: Overview of peptide concentrations as determined by HPLC and resulting peptide ratio grafted to HA.

Sample	LABL or IBR Conc. (nMol)	PLP Conc. (nMol)	Final Ratio
50 kDa SAgA _{LABL} -PLP	475	300	1.5:1
80 kDa SAgA _{LABL} -PLP	396	283	1.4:1
50 kDa SAgA _{IBR} -PLP	297	377	1:1.3
80 kDa SAgA _{IBR} -PLP	262	334	1:1.3

Table 2: Outline of design and statistics of *in vivo* studies

Group	PLP conc. (nMol)	Mw (Da)	Clinical Significance vs. PBS	
			Score	% Weight loss
50 kDa SAgA _{LABL} -PLP 	200	~50000	p< 0.05, Days 14 & 17	n/a
80 kDa SAgA _{LABL} -PLP 		~80000	p< 0.05, Days 14, 17-19	p< 0.05, Days 15-21
50 kDa SAgA _{IBR} -PLP 		~50000	p< 0.05, Days 14, 17-19	p< 0.05, Day 19
80 kDa SAgA _{IBR} -PLP 		~80000	p< 0.05, Days 14, 17-19	p< 0.05, Day 18
PLP-BPI 		~3000	p< 0.05, Days 14 & 17	p< 0.05, Day 16
PBS	0	n/a	n/a	n/a

FIGURES

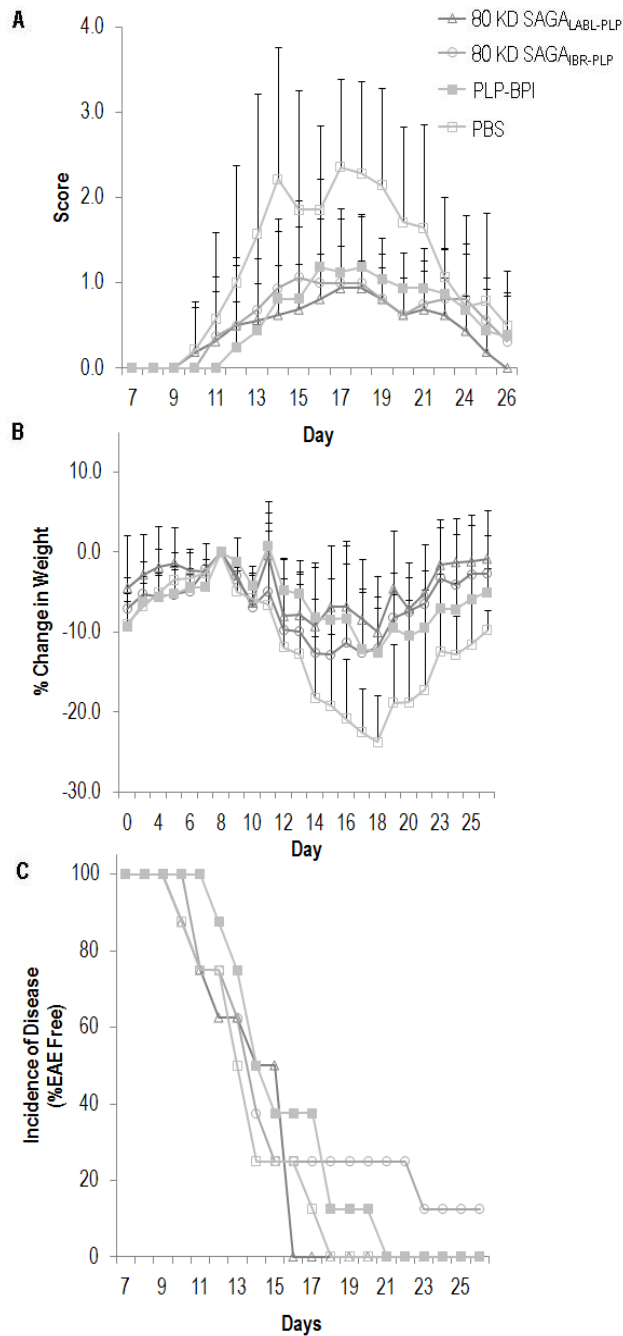


Figure 1: Comparison of clinical performance of SAGA_{ICAM-1}-PLP targeting ICAM-1 and SAGA_{LFA-1}-PLP targeting LFA-1 to negative control (PBS). The data show that SAGAs performed similarly to each other and significantly better than PBS control in (A) clinical disease score, (B) % change in body weight, and (C) incidence of disease. Differences that were statistically significant are summarized in Table 2.

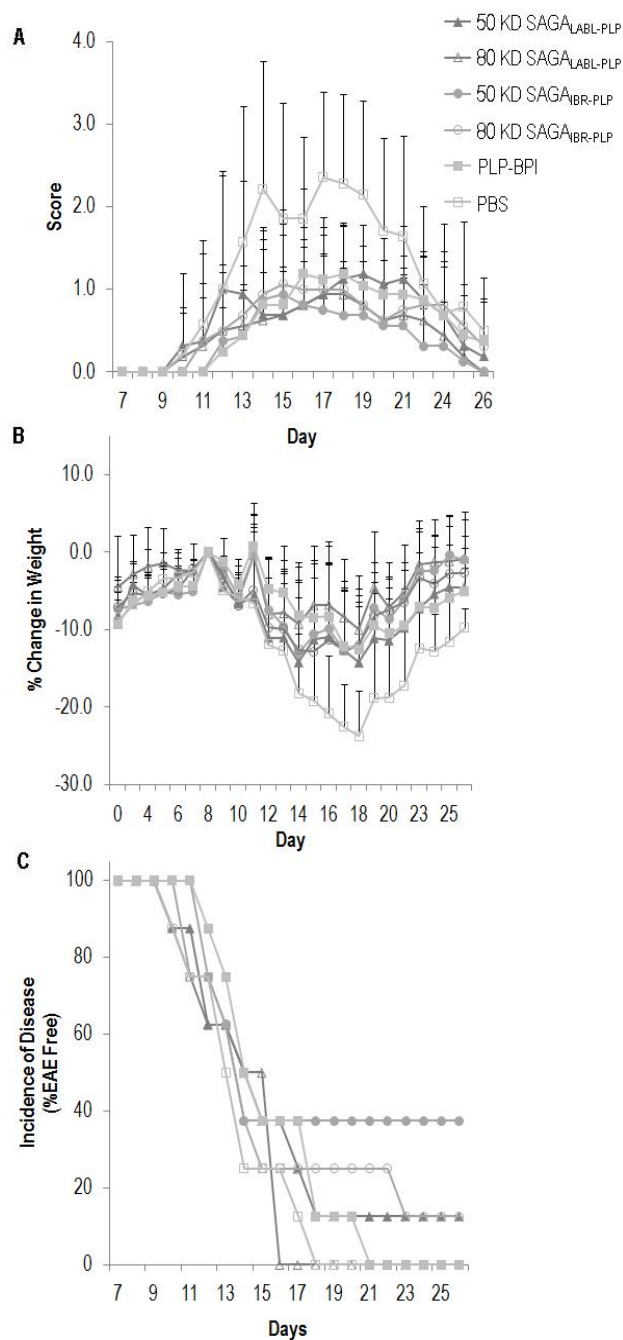


Figure 2: Comparison of clinical performance of two different Mw SAGAs to negative control (PBS). The data show that smaller 50 kDa SAGAs performed significantly better than larger 80 kDa in delaying disease onset. Both SAGAs performed significantly better than PBS control in (A) clinical disease score, (B) % change in body weight, and (C) incidence of disease. Differences that were statistically significant are summarized in Table 2.

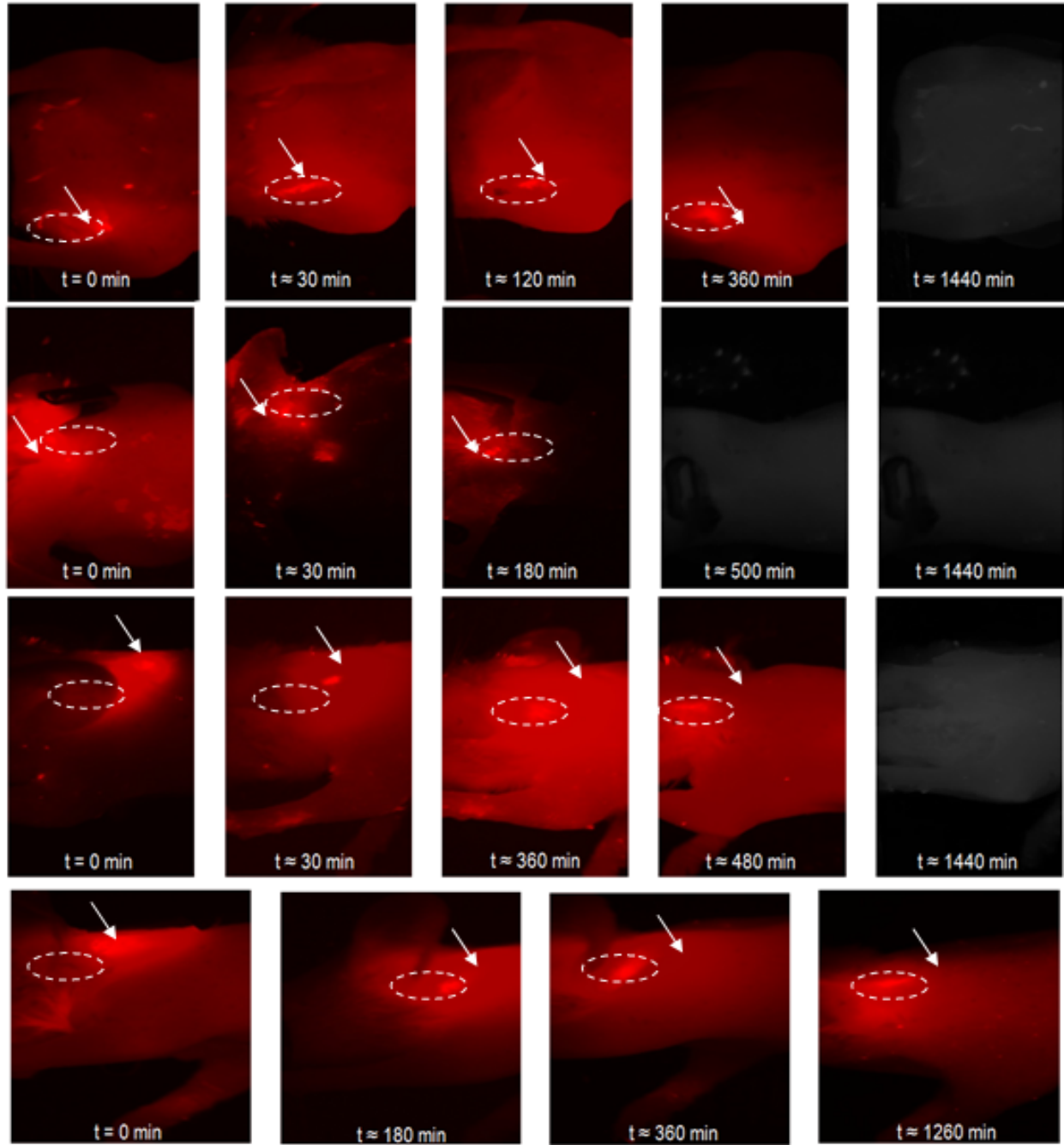


Figure 3: *In vivo* images of mice injected with IR820-HA or IR820-SAGAs. The injection site is indicated by the arrow and the relative location of cervical lymph node packets by the outlined circle. Animals were injected with (A) 35 kDa HA, (B) 70 kDa HA, (C) 50 kDa SAgA_{LABL-PLP}, or (D) 80 kDa SAgA_{LABL-PLP}.

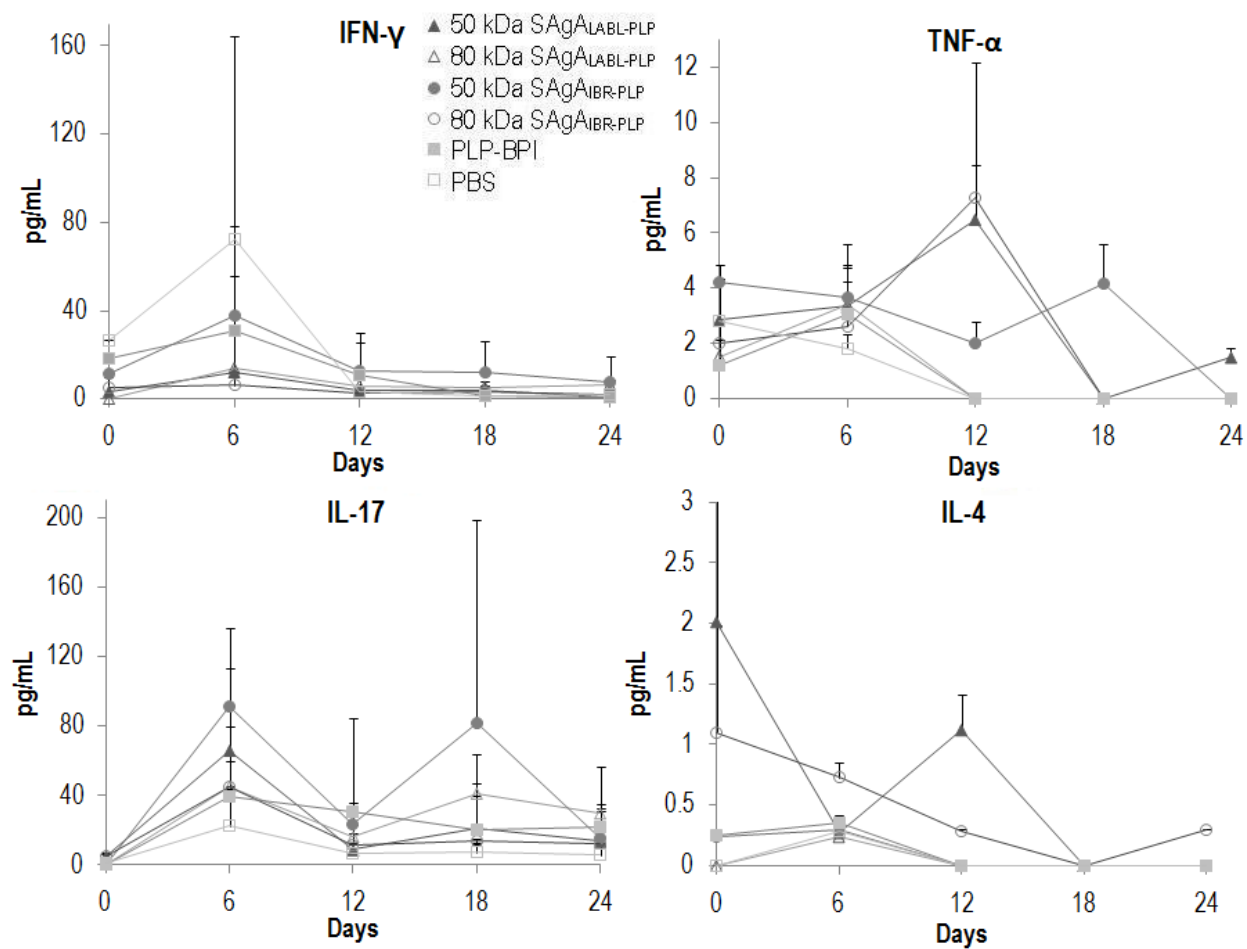


Figure 4: Comparison of cytokine concentration for SAgAs versus controls as determined by ELISA.

Supplementary Tables

Table 1: IR-820 concentration conjugated to HA polymers of 31 and 17 kDa as determined by NMR

Mw	31000	17000
Mw of monomer of HA	379	379
subunits of HA	81.8	44.9
Ref of Integration	245.4	134.6
triplet at 1.18ppm	2.9	2.4
#dyes/subunit	1.4	1.2
#dyes	117.8	53.6
wt%	4.0	5.9

*Also used for synthesis of 50 and 80 kDa SAgAs

Chapter 5

Conclusions and Future Directions

Nanomaterials are unique in that they can be designed to simultaneously engage both physical and chemical immune response pathways. In addition the size, shape, charge, etc. can be modified to compartmentalize nanomaterials to target tissues. This design flexibility has led to the development of unique strategies to modulate immune response. While mechanisms of action may differ, applications using nanomaterials to tailor immune response primarily focus on the antigen presentation profile along the nanomaterial surface. Controlling the number, density, and presentation pattern of antigens are all points of interest.

The goal of this work has been to develop a multivalent nanomaterial that presents both antigen and cell-adhesion inhibitor simultaneously in order to suppress experimental autoimmune encephalomyelitis. HA polymer and PLGA nanoparticles were used as scaffolds to synthesize “antigen arrays,” on which antigen, PLP, and cell-adhesion inhibitor, LABL or IBR, were conjugated using novel *N*-oxime chemistry. These materials were characterized to determine reaction efficiency, ratio of conjugated peptides, and effect of material size/solubility (polymer vs. nanoparticle) on *in vivo* efficacy. Analysis by HPLC demonstrated that *N*-oxime chemistry provided high reaction efficiency for grafting peptides to HA. Additionally, this novel synthetic approach also allowed for simultaneous conjugation of two peptide species in equimolar ratios via a single step reaction. Further analysis showed that these antigen arrays demonstrated conjugate stability at physiological pH. Initial *in vivo* studies showed that the Soluble Antigen Arrays (SAGAs) built on the HA backbone were able to suppress disease progression more significantly than HA or PBS treatments as evidenced by the reduction in clinical score and improved maintenance of body weight. The dose level of SAGAs was optimized and tested against PLGA nanoparticle arrays. While both treatments demonstrated similar results for weight maintenance, only the SAGAs demonstrated significant clinical efficacy.

The effect of co-grafting ICAM-1 or LFA-1 alongside antigen as well as the role of size of the manufactured SAGAs, was also investigated. Clinical scores and weight were monitored and cytokine profiles were collected for animals treated with the various SAGA. The SAGAs

targeting ICAM-1 or LFA-1 both produced similar clinical scores; however, the SAgAs targeting LFA-1 changed the IFN- γ , TNF- α , and IL-17 cytokine profiles compared to SAgAs targeting ICAM-1. This result demonstrated the complex nature of the immune response since similar clinical efficacy was achieved in spite of different cytokine responses. When SAgA size was decreased from 80 kDa to 50 kDa significant differences were seen in the ability of the smaller arrays to delay the time to disease onset. These results were corroborated for both SAgA targeting species. Additionally, the cytokine profiles were altered by this decrease in SAgA Mw with the smaller SAgAs producing higher levels of IFN- γ and IL-17 compared to the larger arrays.

Future work with these SAgAs should further examine the chemical stability of the manufactured materials, optimize the targeting and drainage characteristics (e.g. size, shape, solubility), and investigate the drainage kinetics. Material characterization should focus on both, optimizing the synthesis conditions as well as evaluating the storage and blood plasma stability of the manufactured materials. To date, the synthesis of the materials has been derived from conditions reported in the literature for similar reactions. Reaction efficiency may be increased and reaction time decreased through manipulation of buffer composition, concentration, pH, temperature, or catalyst. Additionally, the purification strategies of the manufactured materials may be optimized to increase product yield. Beyond material manufacture, SAgAs could be evaluated for their blood plasma and long-term storage stability. The studies completed here demonstrated that both cell-adhesion inhibitor and disease-specific antigen should be co-delivered along either a soluble polymer or nanoparticle to achieve clinical success. An understanding of the stability of the materials is crucial in predicting material efficacy.

In addition to understanding the physical stability of the manufactured SAgAs, optimizing the cell receptor target and/or therapeutic size provides options for therapeutic enhancement. Also, the completed studies targeted a 1:1 ratio of cell-adhesion inhibitor: MS antigen while still maintaining the total hapten density as established by “Dintzis rules.” The effect of antigen **or**

cell-adhesion inhibitor number/density should be tested as illustrated in Table 1. Studies completed here demonstrated that polymers displaying only cell-adhesion inhibitor or only antigen did not suppress EAE while a 1:1 ratio provided significant suppression. This suggests that coincident display of both antigen and cell-adhesion inhibitor is necessary; however, the tested 1:1 ratio is not guaranteed to be the optimum. Systematically varying the LABL or IBR and PLP ratio as illustrated in Table 1 may enhance clinical results.

Pilot studies in this thesis investigated the role of co-delivery of cell-adhesion and antigen peptides via the same polymer (SAgA_{LABL-PLP}) as opposed to a mixture of homopolymers (e.g. only LABL or only PLP). Delivery of the homopolymers individually demonstrated no efficacy; however, when delivered as a mixture, disease suppression was achieved similar to the SAgA_{LABL-PLP} and PLP-BPI controls (Figure 1-A). Animals treated with the homopolymer mixture also maintained body weight similar to the controls (Figure 1-B). The presence of the two signals appeared responsible for clinical efficacy without requiring conjugation to the same polymer. To further evaluate this, homopolymers should be injected as a mixture, as well as separately into the same injection site and at different sites.

Lastly, the remaining SAgA characteristic that may provide added efficacy would be the physical size of the final SAgA product. Initial *in vivo* imaging studies suggested that manipulating SAgA size altered the drainage characteristics. Additionally, this slight difference in drainage profile produced significant differences in the clinical scores as well. Clinical efficacy may be correlated to the ability of the material to drain away from the injection site and into the surrounding tissues. It is suspected that relatively rapid transit to the lymph nodes draining the CNS may be an important effect or of response. By manipulating final Mw, the mobility of the synthesized SAgAs is expected to change as outlined in Table 2. After synthesis, each SAgA should be evaluated in the EAE model, using imaging to correlate drainage to clinical efficacy.

The effect of multivalent antigen presentation was preliminarily explored to determine the cross-reactivity of the SAgA therapies. Extended residence time, as suggested by *in vivo* imaging studies, and unique multivalent antigen presentation compelled an initial evaluation of SAgAs displaying non-PLP antigens for treated PLP-induced EAE. The peptide epitope of myelin oligodendrocyte glycoprotein (MOG, A α -GWYRSPFSRVVHL) was conjugated to HA with a previously evaluated cell-adhesion inhibitor (LABL or IBR). In addition, an array displaying antigen only (MOG and PLP) was tested. The MOG SAgAs were then injected into animals with EAE induced using PLP following the procedure outlined in previous chapters. Interestingly, the SAgA_{LABL-MOG} and SAgA_{MOG-PLP} showed decreased clinical scores; however, disease suppression was not significant when compared to PBS (Figure 2-A). These results concurred with the weight maintenance data (Figure 2-B); however, disease onset did not seem to be affected with all mice developing EAE at similar times (Figure 2-C).

SAgA clinical efficacy can be optimized by systematically investigating SAgA physical characteristics such as size, drainage profiles, and antigen presentation motifs. In addition to these physical parameters, evaluation of the optimized SAgAs effect on binding and cytokine production in both *in vitro* and animal models experiments will help to explain the cellular responses to the SAgAs. Collectively, these recommended studies will help to define the mechanisms of action of SAgAs and will offer insights into new design strategies for further improving performance.

TABLES

Table 1: Proposed study to examine the effect of cell-adhesion to antigen ratio.

SAgA	LABL cell-adhesion inhibitor Mol %	PLP antigen Mol %	Outcome
PLP and LABL (variable ratios) grafted to HA	0	100	Limited Suppression
	25	75	Varied Suppression
	50	50	
	75	25	
	100	0	Disease Exacerbation

Table 2: Proposed SAgA to investigate effect of therapeutic Mw.

SAgA	Mw Hyaluronic acid scaffold (kDa)	Theoretical Array Mw (kDa)	Anticipated Drainage Profile
PLP and LABL (1:1) grafted to HA	1	2.9	Rapid drainage, Leakage to circulation
	6.4	16.6	Primarily localized lymphatic uptake
	17	49.7	
	31	80.5	
	75	219.2	Minimal drainage, depot effect
	132	342.7	

FIGURES

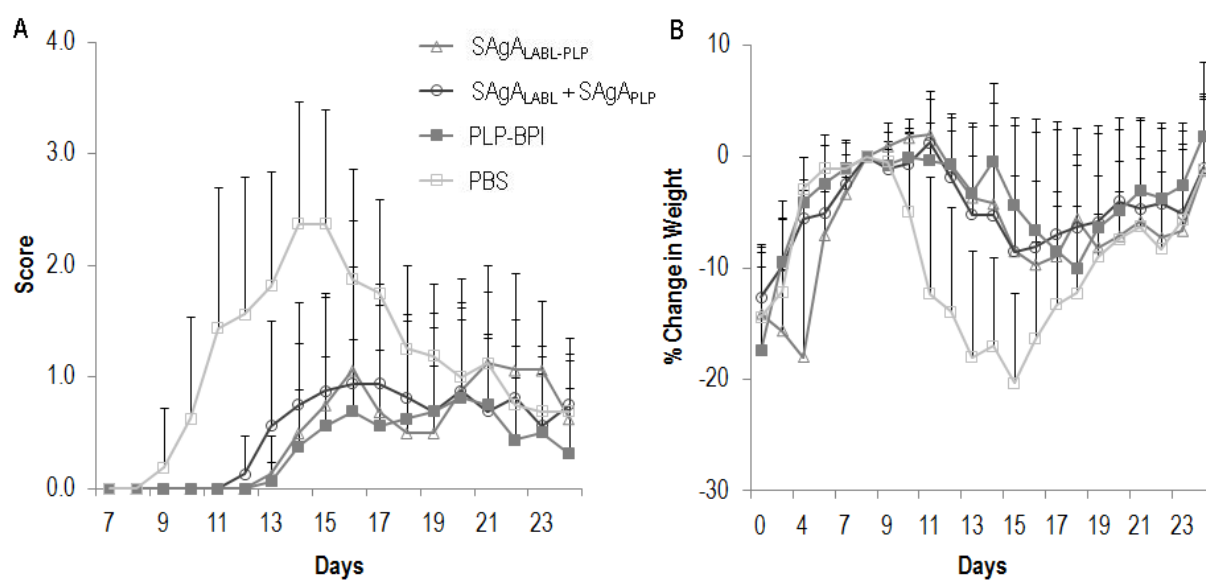


Figure 1: Clinic Comparison of SAg_{LABL-PLP} to a mixture of SAg_{LABL} and SAg_{PLP}. The data suggest the mixture of homopolymers performed similarly to SAg_{LABL-PLP} and PLP-BPI controls in (A) clinical disease score and (B) % change in body weight.

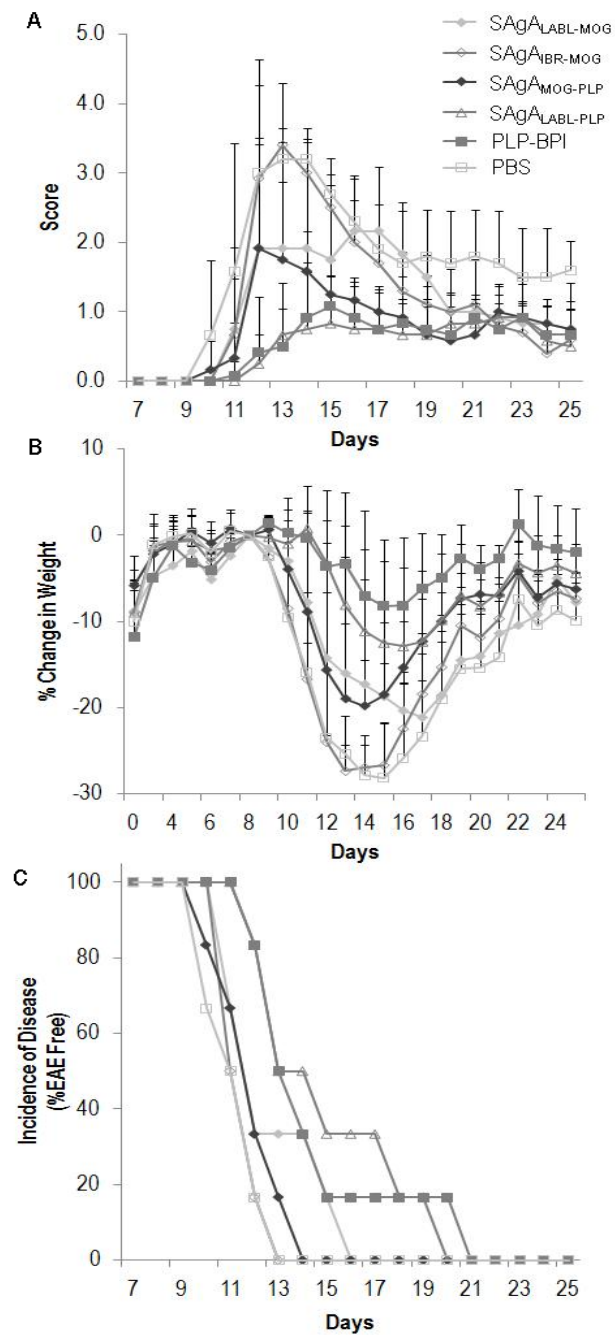


Figure 2: Comparison of clinical performance of SAgAs displaying MOG antigen in PLP induced EAE versus negative control (PBS). The data show that SAgA_{MOG-PLP} and SAgA_{LABL-MOG} performed significantly better than PBS control in (A) clinical disease score, (B) % change in body weight, and (C) incidence of disease.